PROPOSAL TO PAC30

Deeply Virtual Compton Scattering with CLAS at 11 GeV

A. Biselli[†]

Fairfield University, Fairfield, CT 06824, USA

I. Bedlinsky, S. Kuleshov, O. Pogorelko, A. Vlassov

Institute of Theoretical and Experimental Physics, Moscow, 117259, Russia

H. Avakian, V. Burkert, A. Deur, L. Elouadrhiri[†], M. Ito,
M. Vanderhaeghen, R. Niyazov, Yu. Sharabian, and S. Stepanyan

Jefferson Lab, Newport News, VA 23606, USA

V. Baturin, W. Kim[†], S.S. Stepanyan, and M. Yurov

Kyungpook National University, Daegu 702-701, Republic of Korea

V. Mokeev, G. Fedotov, B.S. Ishkhanov, E.L. Isupov, and N.V. Shvedunov

Moscow State University, 119899 Moscow, Russia

M. Amarian, G. Gavalian, C.E. Hyde-Wright, A. Radyshkin, and L. Weinstein

Old Dominion University, Norfolk, VA 23529, USA

V. Kubarovsky and P. Stoler

Rensselaer Polytechnic Institute, Troy, NY 12181, USA

J. Ball, P. Bertin, R. De Masi, M. Garçon, F.-X. Girod,
M. Guidal, M. Mac Cormick, M. Mazouz, B. Michel, S. Niccolai,
B. Pire, S. Procureur, F. Sabatié[†*], E. Voutier, and S. Wallon

LPC (Clermont) / LPSC (Grenoble) / IPNO & LPT (Orsay)

CPhT-Polytechnique (Palaiseau) / SPhN (Saclay)

CEA/DSM/Dapnia & CNRS/IN2P3, France

K. Joo, N. Markov, M. Ungaro, and Bo Zhao

University of Connecticut, Storrs, CT 06269, USA

J. Annand, D. Ireland[†], R. Kaiser, K. Livingston, D. Protopopescu, G. Rosner, and B. Seitz

University of Glasgow, Glasgow G12 8QQ, UK

J. Connel, H. Egiyan[†], M. Holtrop[†], and L. Zana

University of New Hampshire, Durham, NH 03824, USA

C. Djalali, R.W. Gothe, J. Langheinrich, K. Park, S. Strauch, and D. Tedeschi

University of South Carolina, Columbia, SC 29208, USA

N. Baillie, R. Fersch, and K.A. Griffioen

The College of William and Mary, Williamsburg, Virginia 23187, USA

G. Asryan, N. Dashyan, K. Egiyan, N. Gevorgyan, and H. Hakobyan

Yerevan Physics Institute, Yerevan, Armenia 375036

A CLAS collaboration proposal

[†]Co-spokesperson [*]Contact: sabatie@jlab.org

Abstract

We propose two separate experiments that use the reaction $ep \rightarrow ep\gamma$; one to measure the beam-spin asymmetries using an unpolarized target, and one to measure the target-spin asymmetries using a longitudinally polarized target. These observables are linked to the imaginary part of the DVCS amplitude and therefore to specific linear combinations of Generalized Parton Distributions. These two measurements will extend the 6 GeV Hall-B experiments E01-113, E06-003 and E05-114 to both lower and higher x_B (down to 0.1, up to 0.7) and to higher Q^2 (up to 9 GeV^2) with much higher statistics, and will provide a full mapping of the beam-spin asymmetries and target-spin asymmetries over the available kinematic region for an 11 GeV electron beam. The CLAS detector upgrade offers an excellent three-particle acceptance for this reaction, and together with the higher achievable luminosity it will allow for a significant improvement of the statistical accuracy of these measurements. In addition to the single spin asymmetries, the helicity dependent cross sections will also be extracted for specific kinematics and with reasonable systematic uncertainty.

Contents

I. INTRODUCTION

The challenge of understanding the nucleon electromagnetic structure is still going on after five decades of experimental scrutiny. From the initial measurements of elastic form factors to the accurate determination of parton distributions through deep inelastic scattering (DIS), the experiments have increased in statistical and systematic accuracy. Ten years ago a unifying concept for the description of the nucleon structure was introduced, now commonly known as Generalized Parton Distribution (GPD)[1–4]. These functions contain the usual form factors and parton distributions, but in addition they include correlations between states of different longitudinal momentum and transverse momentum dependence. GPDs can therefore give three-dimensional pictures of the nucleon, providing information such as the transverse spatial distribution as a function of the longitudinal momentum fraction of the quarks. With a complete knowledge of these functions, it will be possible to obtain for instance the high and low-momentum components of the nucleon for different flavors. The holy grail of these type of measurements is to provide enough data to determine the total angular momentum carried by quarks through Ji's sum rule [2]

Deeply Virtual Compton Scattering (DVCS) is the simplest and therefore cleanest process which can be described in terms of GPDs. It is the first reaction which allows unambiguous extraction of GPDs from data and provides the cornerstone of their exploration at Jefferson Lab. First results of DVCS Beam Spin Asymmetries (BSA) in Hall B [5] and HERMES [6] in 2001 have suggested that the GPD framework can be applied to a 6 GeV experiment, for which the virtuality of the photon probe is low.

Two dedicated experiments have since taken data: the Hall A E00-110 experiment measured helicity dependent cross sections and provided the best check so far of the Bjorken-type scaling which is expected of DVCS in the factorization regime [7]. With a fair degree of confidence, one can now say that DVCS measurements at Jefferson Lab energies are indeed relevant to the investigation of the GPDs in the valence region. The Hall B E01-113 experiment took data 6 months later, and is currently in the final stages of the analysis [8]. The main goal of that experiment was to perform BSA measurements in a large kinematic domain, scanning this observable as a function of x_B, t and Q^2. Recently new results on the first measurements of the target spin asymmetry were published by the CLAS collaboration [9], confirming again that the factorization is likely to be applicable at Q^2 values as

low as 2 GeV^2. Another experiment E05-114 is planned for CLAS at Jefferson Laboratory in the near future to measure the target spin asymmetries using similar equipment which was used in E01-113 experiment.

With the advent of an 11 GeV beam and an upgraded CLAS, experiments similar to E01-113 and E05-114 will provide even larger kinematical coverage with much improved statistics. CLAS will be in a unique position to explore fully the (x_B, t, Q^2) space with its large acceptance, imposing severe constraints on theoretical models of the nucleon structure.

In this document we propose to carry out two separate experiments, in two different experimental configurations, utilizing separate beam times. The first is a measurement of the beam spin asymmetries of electron scattering from an unpolarized liquid hydrogen target. The second experiment is dedicated to measuring target spin asymmetries using a longitudinally polarized target. Because the physics motivation and the theoretical formalisms related to both proposals are common, we presented a single sections for the physics motivation and experimental techniques common for both experiments. The discussions of the accuracy of the proposed experiments and the required beam time are presented in separate sections for each proposal.

II. THEORY AND MOTIVATION

A. Brief overview of Generalized Parton Distributions

Almost 10 years ago, Ji, Radyushkin and others[1–4, 10] showed that the DVCS reaction $\gamma^* p \to \gamma p$ can, in the Bjorken limit, be factorized into a hard scattering kernel and a non-perturbative part, containing information about the electromagnetic structure of the nucleon: the Generalized Parton Distributions. This factorization of the DVCS reaction is represented in Fig.1, where the virtual photon scatters on a single quark, which almost instantly re-emits a real photon. The quark is then inserted back into the nucleon, which is kept intact. In kinematical terms, this factorization is valid when the virtuality of the incoming photon is large ($Q^2 = -q^2$, with q the virtual photon 4-vector, defines the scale of the probe) but the transfer to the nucleon small compared to this scale ($-t << Q^2$). The soft structure of the nucleon is parametrized at twist-2 level by four GPDs: E, H, $\widetilde{E}$ and $\widetilde{H}$.

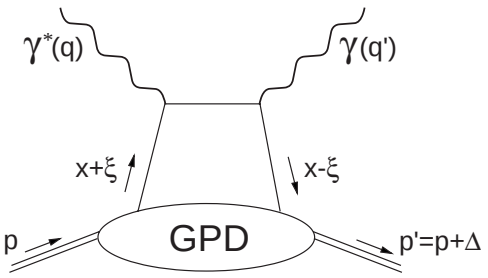

FIG. 1: Handbag diagram to the DVCS process. See text for definition of variables.

All four GPDs depend on 3 variables: x, ξ and t. x characterizes the average light-cone momentum fraction of the struck quark in the loop (not directly accessible experimentally). ξ is the longitudinal momentum fraction of the transfer to the proton $\Delta = p - p'$ (where p and p' are the initial and recoil proton 4-vectors). It reduces to $\xi = x_B/(2 - x_B)$ in the Bjorken limit of infinite Q^2, with x_B the usual DIS variable defined as $x_B = Q^2/(2p \cdot q)$. Finally, $t = \Delta^2$ is the standard Mandelstam variable representing the momentum transfer between the virtual and real photons (or between the target and the recoil proton).

The scale evolution of the GPDs (Q^2-dependence) has been worked out to next-to-leading order of α_S. The Fourier transform of GPDs with respect to $\vec{\Delta}_T$ (the transverse component of Δ) gives access to the (transverse) spatial distribution of partons, as a function of x.

In the forward direction ($\xi = t = 0$), the GPDs H and $\widetilde{H}$ reduce to the usual parton distributions $q(x)$ and $\Delta q(x)$:

$$H^q(x, \xi = 0, t = 0) \; = \; q(x)\,, \tag{1}$$

$$\widetilde{H}^q(x, \xi = 0, t = 0) \; = \; \Delta q(x)\,, \tag{2}$$

where q stands for the quark flavor. The first moments of the GPDs and the elastic form factors are related by the following relations:

$$\int_{-1}^{+1} dx H^q(x, \xi, t) \; = \; F_1^q(t)\,, \qquad \int_{-1}^{+1} dx E^q(x, \xi, t) = F_2^q(t)\,, \tag{3}$$

$$\int_{-1}^{+1} dx \widetilde{H}^q(x, \xi, t) \; = \; g_A^q(t)\,, \qquad \int_{-1}^{+1} dx \widetilde{E}^q(x, \xi, t) = h_A^q(t)\,, \tag{4}$$

where F_1^q and F_2^q are the Dirac and Pauli form factors, g_A^q is the axial form factor and h_A^q is the induced pseudoscalar form factor. Note that the ξ dependence drops out in the integrals.

The second moment of the GPDs is relevant to the nucleon spin structure. It was shown

in Ref. [2] that there exists a gauge-invariant decomposition of the nucleon spin:

$$\frac{1}{2} = J_q + J_g \,, \tag{5}$$

where J_q and J_g are respectively the total quark and gluon angular momentum contributions to the nucleon spin. J_q can be decomposed in a spin part $\Delta\Sigma$ and an orbital momentum part L_q as follows:

$$J_q = \frac{1}{2}\Delta\Sigma + L_q \,. \tag{6}$$

The second moment of the GPDs and the total angular momentum carried by quarks are related via Ji's sum rule:

$$\sum_q \frac{1}{2}\int_{-1}^{+1} dx\, x[H^q(x,\xi,t=0) + E^q(x,\xi,t=0)] = J_q \,. \tag{7}$$

Since $\Delta\Sigma$ is constrained in DIS experiments, if one makes enough measurements to extract the second moments of the GPDs, the sum rule will determine the quark orbital momentum contribution to the nucleon spin.

B. DVCS asymmetries to access GPDs

The $ep \to ep\gamma$ process can either occur by radiation along one of the electron lines (Bethe-Heitler) or by emission of a real photon by the nucleon (DVCS) as shown in Fig. 2. The total cross section is given by [11]:

$$\frac{d\sigma^{ep\to ep\gamma}}{dx_B dy d\Delta^2 d\varphi} = \frac{\alpha^3 x_B y}{16\pi^2 Q^2\sqrt{1+\epsilon^2}} \left|\frac{\mathcal{T}}{e^3}\right|^2 \,, \tag{8}$$

where $\epsilon = 2x_B M/Q$, y is the fraction of the electron energy lost in the nucleon rest frame and the φ is the angle between the leptonic plane (e, e') and the photonic plane (γ^*, γ).

The total amplitude $\mathcal{T}$ is the superposition of the BH and DVCS amplitudes:

$$|\mathcal{T}|^2 = |\mathcal{T}_{BH}|^2 + |\mathcal{T}_{DVCS}|^2 + \mathcal{I} \tag{9}$$

$$\mathcal{I} = \mathcal{T}^*_{DVCS}\mathcal{T}_{BH} + \mathcal{T}_{DVCS}\mathcal{T}^*_{BH} \,, \tag{10}$$

where $\mathcal{T}_{DVCS}$ and $\mathcal{T}_{BH}$ are the amplitudes for the DVCS and Bethe-Heitler processes, and $\mathcal{I}$ denotes the interference between these amplitudes. The individual contributions to the

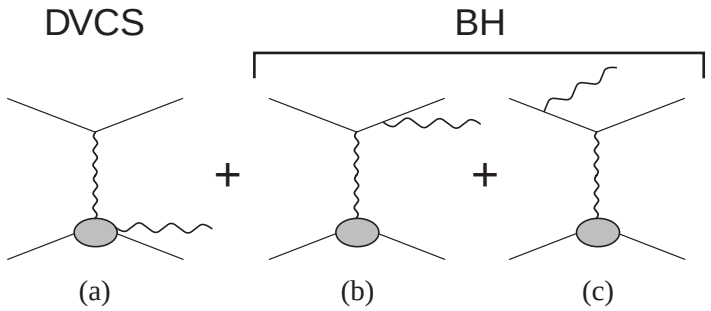

FIG. 2: Diagrams contributing to the electroproduction of a real photon. The DVCS process (a) is shown along with the interfering Bethe-Heitler diagrams (b) and (c).

total $ep \to ep\gamma$ cross section can be written as (up to twist-3 contributions) [11]:

$$|\mathcal{T}_{BH}|^2 = \frac{\Gamma_{BH}(x_B, Q^2, t)}{\mathcal{P}_1(\varphi)P_2(\varphi)} \left\{ c_0^{BH} + \sum_{n=1}^{2} c_n^{BH} \cos(n\varphi) + s_1^{BH} \sin\varphi \right\}, \tag{11}$$

$$|\mathcal{T}_{DVCS}|^2 = \Gamma_{DVCS}(x_B, Q^2, t) \left\{ c_0^{DVCS} + \sum_{n=1}^{2} [c_n^{DVCS} \cos(n\varphi) + s_n^{DVCS} \sin(n\varphi)] \right\}, \tag{12}$$

$$\mathcal{I} = \frac{\Gamma_I(x_B, Q^2, t)}{\mathcal{P}_1(\varphi)P_2(\varphi)}] \left\{ c_0^I + \sum_{n=1}^{3} [c_n^I \cos(n\varphi) + s_n^I \sin(n\varphi)] \right\}, \tag{13}$$

where $\mathcal{P}_1(\varphi)$ and $\mathcal{P}_2(\varphi)$ are the BH electron propagators and can be written as:

$$Q^2\mathcal{P}_1 = (k - q')^2 = Q^2 + 2k \cdot \Delta\,, \tag{14}$$

$$Q^2\mathcal{P}_2 = (k - \Delta)^2 = -2k \cdot \Delta + \Delta^2\,. \tag{15}$$

Note that in Eq.11-13, all $\sin(n\varphi)$ coefficients depend on the beam helicity λ (they disappear in the cross section).

Using either a polarized beam or a polarized target, two separate quantities can be extracted: the **difference of cross section** for opposite beam helicities or opposite target spin, and the **total cross section**, which can be written respectively as:

$$d\sigma^{\rightarrow} - d\sigma^{\leftarrow} = 2 \cdot \mathcal{T}_{BH} \cdot Im(\mathcal{T}_{DVCS}) + \left[|\mathcal{T}^{\rightarrow}_{DVCS}|^2 - |\mathcal{T}^{\leftarrow}_{DVCS}|^2 \right], \tag{16}$$

$$d\sigma^{\rightarrow} + d\sigma^{\leftarrow} = |T_{BH}|^2 + 2 \cdot \mathcal{T}_{BH} \cdot Re(\mathcal{T}_{DVCS}) + |T_{DVCS}|^2\,, \tag{17}$$

where the arrows correspond to either the beam helicity (unpolarized target) or the target spin (unpolarized beam, longitudinally polarized target). At low energy, $|T_{DVCS}|^2$ is predicted to be smaller than other contributions, especially in the cross section difference.

In the total cross section however, this term may be sizeable at small y values. The data collected so far do not have sufficient statistical accuracy to resolve slight differences in the form of the angular distribution of the DVCS-BH interference and $|T_{DVCS}|^2$ terms. Therefore, we do not keep the $|T_{DVCS}|^2$ term in our discussion. On the other hand, it may be possible to make empirical estimates of the relative magnitude of the $|T_{DVCS}|^2$ term using future accurate data. Neglecting the $|T_{DVCS}|^2$ term, the previous equations now simplify to:

$$d\sigma^{\rightarrow} - d\sigma^{\leftarrow} = 2 \cdot \mathcal{T}_{BH} \cdot Im(\mathcal{T}_{DVCS}) \,, \tag{18}$$

$$d\sigma^{\rightarrow} + d\sigma^{\leftarrow} = |T_{BH}|^2 + 2 \cdot \mathcal{T}_{BH} \cdot Re(\mathcal{T}_{DVCS}) \,. \tag{19}$$

As we will detail further, depending on whether the beam helicity or target spin is flipped, different GPD contributions enter the cross section difference. From these two natural observables, one can write asymmetries which are experimentally easier to determine:

$$A = \frac{d\sigma^{\leftarrow} - d\sigma^{\rightarrow}}{d\sigma^{\leftarrow} + d\sigma^{\rightarrow}} \simeq \Gamma_A(x_B, Q^2, t) \frac{s_1^I \sin\varphi + s_2^I \sin(2\varphi)}{c_0^{BH} + c_0^I + (c_1^{BH} + c_1^I)\cos\varphi} \,, \tag{20}$$

where Γ_A is a known kinematical prefactor. Only the twist-3 contribution in the numerator have been included in this, since twist-3 contributions coming from the denominator are kinematically suppressed. If one further neglects higher order harmonics suppressed by $\sqrt{-t}/Q$ or more, we are left with:

$$A \simeq \Gamma_A \frac{s_1^I}{c_0^{BH}} \sin\varphi \,, \tag{21}$$

where c_0^{BH} is again fully calculable, and s_1^I contains twist-2 GPD information. One should be careful with approximations leading to this expression. When trying to estimate GPDs at the 10% accuracy level or higher, it is valid to proceed with these simplified equations at reasonably high Q^2 and low t. However, with the goal of providing accurate GPD measurement at 5% accuracy level or lower, one should not neglect all the other contributions in the final analysis.

In the unpolarized target case, s_1^I can be written in terms of Compton Form Factors (CFF), which are the complex counterparts of GPDs as defined in [11]:

$$s_{1,unp}^I = Im\left\{ F_1\mathcal{H} + \frac{x_B}{2-x_B}(F_1+F_2)\widetilde{\mathcal{H}} - \frac{t}{4M^2}F_2\mathcal{E} \right\} \,, \tag{22}$$

where the *unp* subscript refers to an unpolarized target.

In the longitudinally polarized (LP) target case, s_1^I can be written as a function of the same CFFs:

$$s_{1,LP}^I = Im\left\{F_1\widetilde{\mathcal{H}} + \frac{x_B}{2-x_B}\left(F_1+F_2\right)\left(\mathcal{H}+\frac{x_B}{2}\mathcal{E}\right) - \frac{x_B}{2-x_B}\left(\frac{x_B}{2}F_1 + \frac{t}{4M^2}F_2\right)\widetilde{\mathcal{E}}\right\}. \tag{23}$$

It is instructive to write the CFF $\mathcal{H}$ as a function of GPDs:

$$\mathcal{H}(\xi,t) = \sum_q \left[\frac{e_q}{e}\right]\ \left\{\ i\pi\left[H^q(\xi,\xi,t) - H^q(-\xi,\xi,t)\right]\right.$$
$$\left. +\ \mathcal{P}\int_{-1}^{+1} dx\left[\frac{1}{\xi-x} - \frac{1}{\xi+x}\right]H^q(x,\xi,t)\right\}, \tag{24}$$

where the sum is made over quark flavors q, e_q being their charge. Similar expressions can be written for all CFFs/GPDs. Since $s_{1,unp}^I$ and $s_{1,LP}^I$ both depend on the imaginary part of the CFFs, they directly depend on linear combinations of 3 GPDs at the particular kinematical lines $x = \pm\xi$. On the contrary, the real part of the CFFs, and therefore this principal part integral over x of GPDs can only be accessed in a clean way through beam charge asymmetry. The real part of the CFFs also enters the total cross section but their disentanglement is made very complicated by the presence of $\mathcal{T}_{DVCS}^2$ terms which cannot be separated easily and is of the same order of magnitude. In Fig. 3 dependence of the proton GPDs H, $\widetilde{H}$, and E on ξ, for $x = \xi$ point and for four values of transferred momentum t, are shown.

The main contribution to $s_{1,unp}^I$ is $F_1\mathcal{H}$ and again, this approximation can be used to give orders of magnitude estimates of $\mathcal{H}$ from data but not to extract the GPD accurately. The main contributions to $s_{1,LP}^I$ come from both $\mathcal{H}$ and $\widetilde{\mathcal{H}}$, whereas the $\widetilde{\mathcal{E}}$ contribution is suppressed.

It becomes obvious that in order to extract GPDs with good accuracy, an extensive program covering a large kinematical domain, with high precision data in both asymmetries and cross section measurements is absolutely necessary. The extraction of GPDs will be done in the same manner as Parton Distribution Functions are extracted from structure function measurements, by means of a global fit of data using GPD parametrizations.

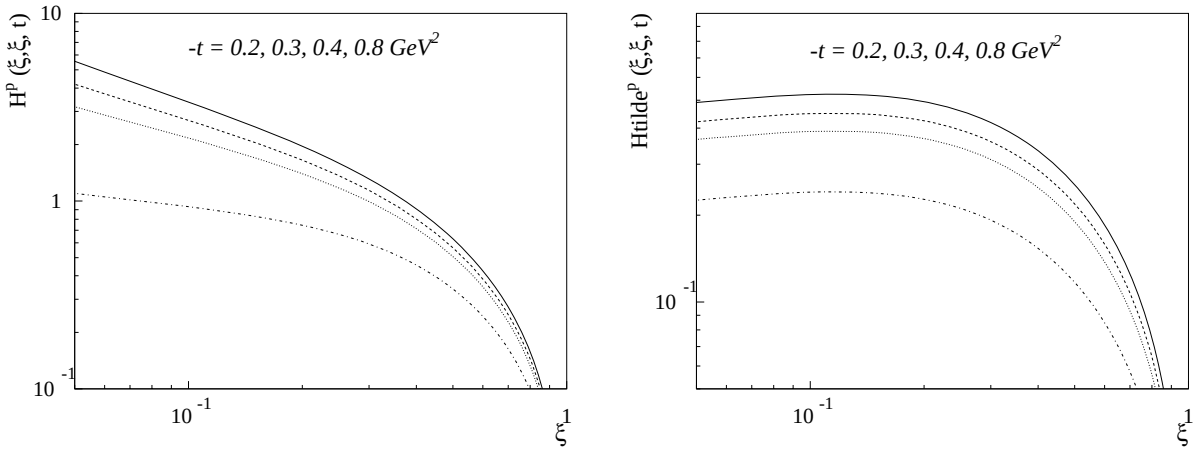

FIG. 3: The ξ dependence of proton GPDs H (left) and $\widetilde{H}$ (right) for the particular kinematical line $x = \xi$. The solid lines are for $-t = 0.2$ GeV^2, the dashed lines are at $-t = 0.3$ GeV^2, the dotted lines are at $-t = 0.4$ GeV^2, and the dashed-dotted lines are at $-t = 0.8$ GeV^2.

III. EXPERIMENTAL SITUATION

This section gives a short overview of DVCS experiments on the proton (BSA, TSA, cross-sections), focusing on data already published or shown in conference, as well as proposals or intentions for significant contributions to the GPD field. All these contributions are listed in Table I and summarized in the following subsections.

A. Published and preliminary data on DVCS

The first published DVCS beam spin asymmetry data came at the same time from HERMES and Hall B. The Hall B measurement used CLAS at 4.2 GeV electron energy [5]. In that experiment, only the electron and proton were detected, while the photon was inferred using the missing mass technique. The π^0 background was subtracted globally using a 2-gaussian fit to the missing mass spectrum. To get sufficient statistical accuracy, data were integrated over the full CLAS acceptance. Resulting average kinematical variables were: $< x_B >= 0.19$, $< Q^2 >= 1.25$ GeV^2, $< -t >= 0.19$ GeV^2. The φ dependence of the BSA could be reasonably fit by a sine wave of amplitude 0.202 $\pm$0.03 (stat+syst). This measurement triggered the experimental interest in DVCS in Hall B.

HERMES published its own BSA, using a positron beam on an unpolarized target (end-of-fill runs) [6]. In that experiment, only the positron and photon were detected, and the proton was inferred by the missing mass technique. Exclusivity was checked by a Monte-Carlo method. To get sufficient statistical accuracy, data were integrated over the full HERMES acceptance. Resulting average kinematical variables were: $< x_B >= 0.11$, $< Q^2 >= 2.6$ GeV^2, $< -t >= 0.27$ GeV^2. The φ dependence of the BSA could be reasonably fit by a sine wave of amplitude 0.23 $\pm$0.05 (stat+syst).

Fairly recently, earlier CLAS data were used to extract the target spin asymmetry [9]. These measurements were carried out using CEBAF 5.7 GeV electron beam incident on a longitudinally polarized target. The φ dependence of the measured target asymmetry is consistent with the assumption that the handbag diagram is the dominant term in the virtual Compton scattering amplitude. The CLAS measurement yielded $A_{UL}^{\sin\varphi} = 0.252 \pm 0.042^{stat} \pm 0.020^{sys}$ value for $\sin\varphi$ component for the target spin asymmetry at $< Q^2 >= 1.82$ GeV, $< x_B >= 0.28$ and $< -t >= 0.31$ GeV^2.

The HERMES collaboration recently reported a measurement [12] of the target spin asymmetries at average $< Q^2 >= 2.5$ GeV^2, $< -t >= 0.12$ GeV^2 and $< x_B >= 0.1$.

	BSA	TSA
Non-dedicated experiments (published or submitted)	CLAS [5] HERMES [6]	CLAS [9]
Dedicated experiments (performed 2004-2005)	Hall A E00-110 CLAS E01-113	
Dedicated experiments (approved 2006-2008)	HERMES CLAS E06-003	CLAS E05-114
Projects (after 2010)	COMPASS Hall A CLAS12 (this proposal)	CLAS12 (this proposal)

TABLE I: Summary of DVCS experiments (on proton target), performed or planned measurements

The preliminary estimates for the $\sin\varphi$ moment of the target beam spin asymmetry is $A_{UL}^{\sin\varphi} = -0.071 \pm 0.034^{stat}$.

The CLAS experiment E01-113 [8] took data in 2005 and very recently showed its first preliminary results. More details about this experiment are discussed in Section IV. Concurrently, analyses from other non-dedicated CLAS running periods are in progress [13, 14].

The Jefferson Lab Hall A experiment E00-110 [7] took data in 2004 and measured the helicity-dependent cross-sections for DVCS at $Q^2 = 1.4, 1.9$ and 2.3 GeV^2, at fixed $x_B = 0.36$, as a function of t and φ. As mentioned in the introduction, the Q^2-dependence of the twist-2 component in the difference of cross sections for electrons of opposite helicity was shown to follow the predicted handbag dominance scaling. Moreover, the twist-3 component is very much suppressed compared to twist-2, giving the best proof so far that the GPD formalism is applicable at energies accessible to Jefferson Lab, even pre-upgrade. Note that the E03-106 experiment in Hall A [15] using the same experiment but with a deuterium target took data immediately after E00-110. The analysis is more complicated than for the proton data, but preliminary results on neutron DVCS are especially encouraging.

B. Proposals

The experiment E05-114 [16] aimed at measuring the target spin asymmetry in a larger kinematic domain with higher statistics was proposed to PAC28 and approved with an "A" rating. That experiment is planned to run in 2008. The second half of experiment E01-113 (unpolarized DVCS on proton), called E06-003 [17], is also planned for 2008, and will more than double the statistical accuracy of the current data.

HERMES will run in 2006-2007 with the addition of a recoil detector, allowing the detection of the proton, therefore putting stronger constraints on exclusivity requirements.

The COMPASS experiment at CERN is currently investigating the possibility of running a DVCS experiment after the muon and hadron runs planned for the next few years [18]. This experiment will access lower x_B than JLab or HERMES data, probing the largely unknown gluon sector. A formal letter of intent is planned for the next year.

IV. REVIEW OF E01-113 TECHNIQUES AND RESULTS

A dedicated DVCS experiment already ran in the Hall B of Jefferson Lab in the spring of 2005. This experiment was initially approved by PAC-20 with "A" rating. The goals of the experiment were the measurement of the t and x_B dependence of beam spin asymmetry for several Q^2 bins and the extraction of the helicity-dependent cross section difference in the reaction $ep \to ep\gamma$. As CLAS covers a broad kinematical, the experiment will test the Q^2 dependence of the DVCS process for different x_B. This will test whether we are in a regime where a direct interpretation of the results in terms of GPDs is possible.

The first part of the experiment was completed during March-May of 2005. A 5.75 GeV longitudinally polarized electron beam with an average polarization of $\sim 80\%$ was used, incident on the 2.5 cm long liquid hydrogen target. As a trigger for the data acquisition of CLAS, the coincidence signal of the forward electromagnetic calorimeter (EC) and the Cherenkov counter (CC) was used. About 43% of the total required data for the beam spin asymmetry measurement were collected. In Fig. 4, the kinematical coverage in Q^2, x_B, and t for reconstructed (e, p, γ) events from the preliminary analysis of the collected data is shown.

The E01-113 configuration was very similar to the one proposed here. All three final-state particles from the reaction $\vec{e}p \to ep\gamma$ were detected. The same inner calorimeter (IC) to be used in this experiment was installed for the detection of high-energy photons in the angular range from 4 to 16 degrees, while a new superconducting solenoid magnet was used to shield the CLAS drift chambers (DC) and IC from Møller electrons.

The same type of simulations as used in these proposals were very successfull at describing the background in the IC, originating mostly from Møller electrons. As anticipated, only the inner crystal layer suffered from significant pile-up and exhibited a small gain loss over a three-month period (see Fig. 5).

The experiment E01-113 then took data at the designed luminosity of 2×10^{34} cm^{-2}sec^{-1}, limited mostly by instantaneous rates and current in the drift chambers.

In these proposals, the magnetic field configuration will be different, with a stringe-field extending much further away, and the IC located at a larger distance from the target. The success in simulating the background in E01-113 gives us confidence in both the present simulations and the new configuration proposed for CLAS12.

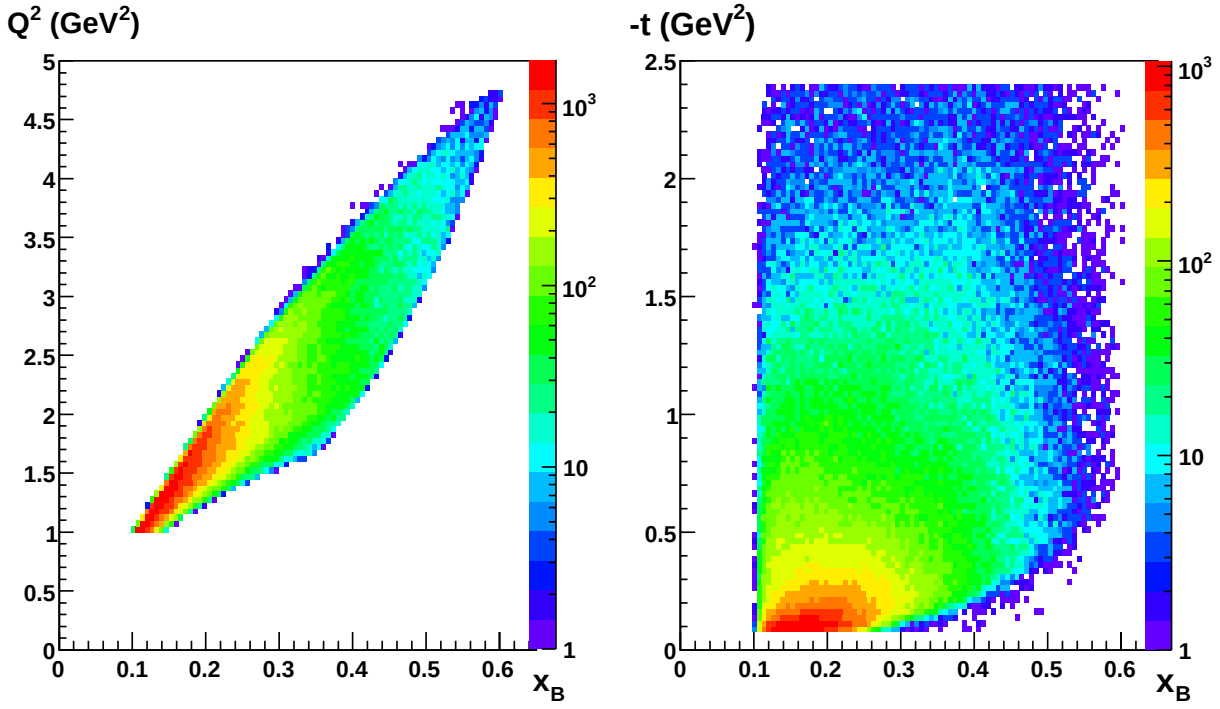

FIG. 4: The Q^2, x_B, and t coverage during the spring 2005 DVCS run with CLAS at 5.75 GeV beam energy.

A. IC performance

- Energy resolution The calorimeter was calibrated using two-cluster events from $\pi^0 \to \gamma\gamma$ [19]. The obtained mass resolution of 7 MeV (σ) translates into an energy resolution of 4.5% for 1 GeV photons. With additional information from simulation [20] and from preamplifier noise, our estimate of the energy dependence of this resolution is

$$\frac{\sigma_E}{E}(\%) \sim \frac{1.9}{E} \oplus \frac{3.3}{\sqrt{E}} \oplus 2.4 \tag{25}$$

  When extrapolated to 6-9 GeV photons, the resolution will be dominated by the constant term.

- Position resolution The intrinsic IC position resolution, as estimated from simulation [20] and compatible with present data, is

$$\sigma_x = \sigma_y(\text{mm}) \simeq \frac{1.8}{\sqrt{E}} \oplus 0.1 \tag{26}$$

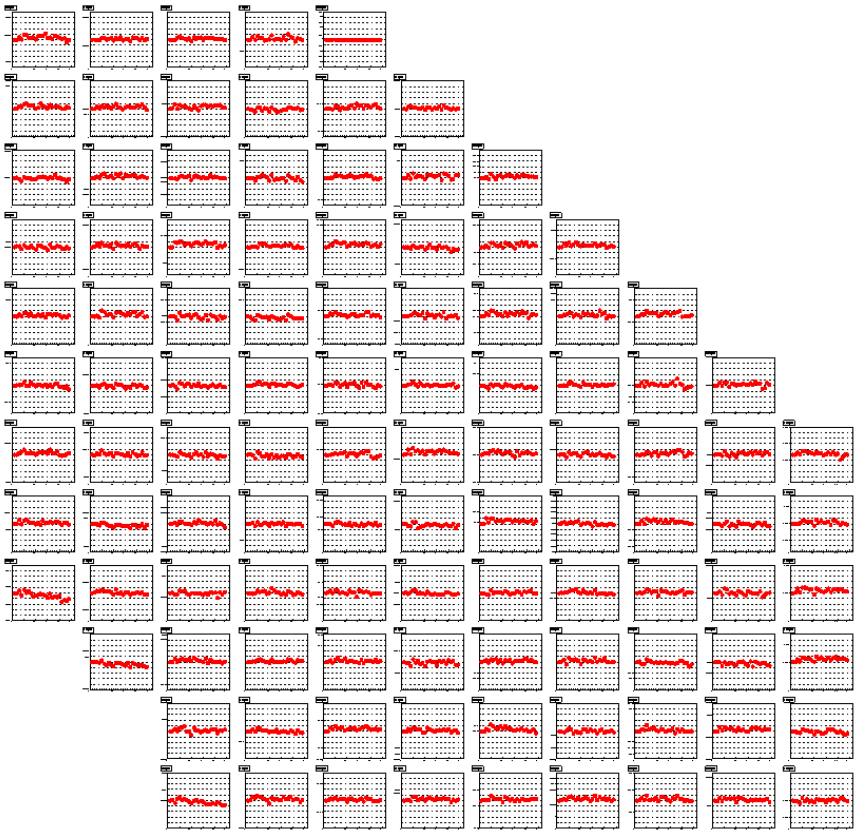

FIG. 5: Gain variations for each IC crystal in the upper right quadrant, as a function of time over the whole run, as measured by the laser monitoring system. Dashed horizontal lines are separated by 5%.

This will translate into .2 mrad resolution for a 9 GeV photon for a point target viewed from a 1.75 m distance.

- Time resolution After electron flight path correction and time-walk correction, a resolution of 0.7 ns was obtained in the $e - \gamma$ coincidence [21]. This is dominated by the multihit-TDC channel width of 0.5 ns. This resolution may be used to reject the few remaining accidentals in the CLAS-IC coincidence.

B. Measurement of radiation damage in the IC

In anticipation of a long term operation of the inner calorimeter, radiation damage was both simulated beforehand [22] and measured during the spring 2005 run. For this purpose,

pedestal runs were taken with beam on, and the excess energy above the pedestal peaks analyzed and translated into radiation dose. The results for the central part of IC are illustrated in Fig. 6. The observed distributions are in reasonable agreement with simulations. The inner ring crystals were obviously the most subject to radiation, at a level approaching estimates for LHC/CMS operation. Only for these did we observe a few percent decrease of signal output over the whole run period. We can then operate the inner calorimeter anew and for longer periods of time with a comparable background level.

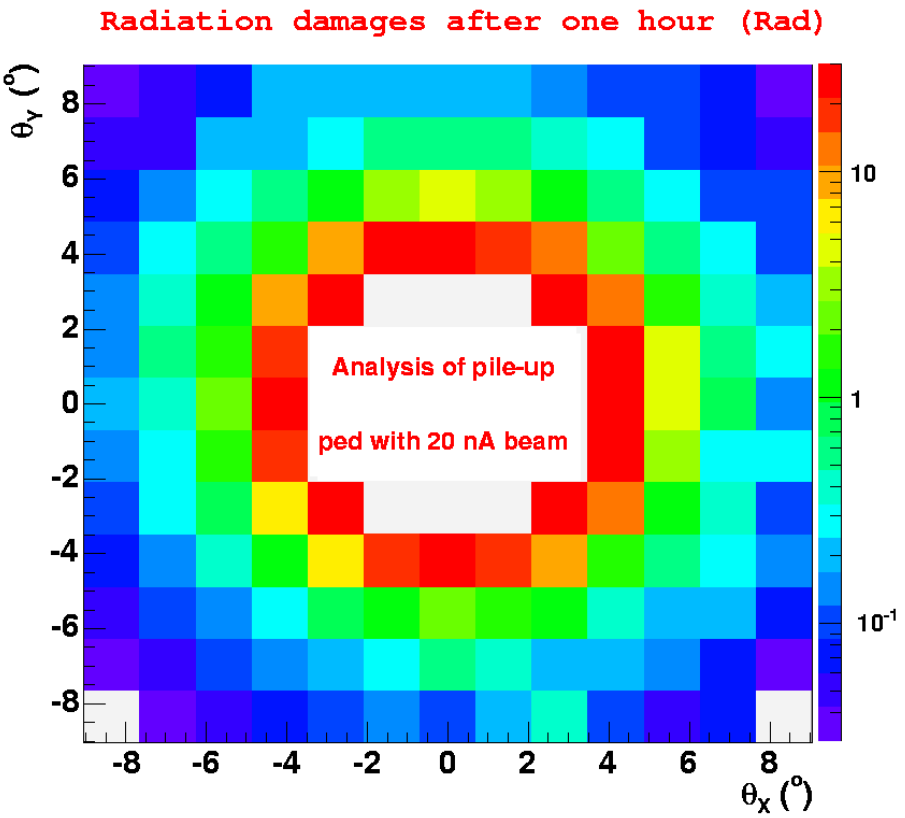

FIG. 6: Radiation dose, in rad per hour, for the central part of IC. Each square corresponds to an IC crystal.

C. Preliminary results

After calibration of all detector subsystems and particle identification cuts for the scattered electron and proton, the selection of the $ep \to ep\gamma$ events is straightforward. Requiring a good electron trigger, a proton and at least one photon above 1 GeV, the $ep \to ep\gamma$ events

appear as a clear peak in all variables expressing a kinematical constraint. For example, Fig. 7 gives the angular constraints, the missing momentum in both transverse directions, the missing energy for $ep \to ep\gamma X$ and the missing mass for $ep \to e\gamma X$. The red curves, obtained after a cut on the missing transverse momentum, show a distinct $ep\gamma$ peak (indeed cleaner than in any other DVCS experiment). Note that simulations indicate that a residual π^0 contamination is still possible after this selection, corresponding to asymmetric π^0 decays where a low-energy photon was not detected.

After putting a cut on the missing energy spectrum, the "raw" asymmetries are easily extracted. Fig. 8 gives a good indication of the resulting statistical precision over a wide kinematical range. This figure contains about 700,000 events, in accordance with E01-113 estimates.

These preliminary results illustrate the event selectivity when detecting the three particles in the final state, and are a good example of what is to be obtained with a large acceptance spectrometer. With increased luminosity and statistics, and over even a wider kinematical range in Q^2 and x_B (and with a finer binning in t), not only very stringent constraints on any GPD model or parameterization can be imposed, but also global fits can be performed.

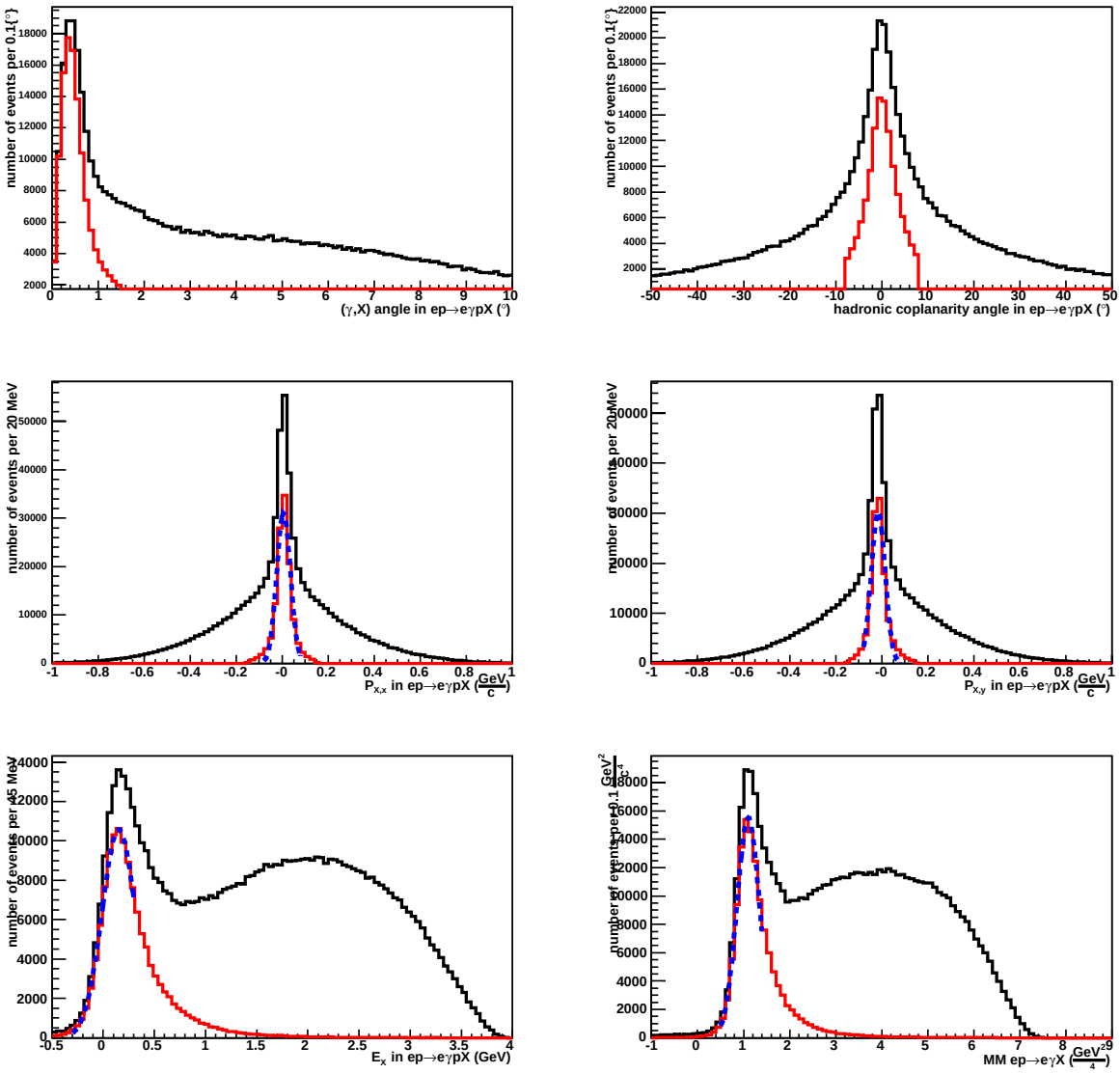

FIG. 7: E01-113 data; Top: cone angle (between γ and X in $ep \to epX$) and coplanarity angle (plane $\gamma^*\gamma p$); Middle and bottom: missing transverse momenta and energy for the $ep \to ep\gamma X$ configurations (with γ in IC), followed by missing mass squared for $ep \to e\gamma X'$, still for the same detected configurations. The last two graphs show peaks shifted from the expected position, presumably due calibration issues still to be addressed. The red curves are obtained after a cut $\Delta P_x^2 + \Delta P_y^2 < (0.15 \text{ GeV})^2$ and angle cuts (resp. 1.5° and $\pm 8^\circ$) on the top histograms (the two sets of cuts are highly correlated).

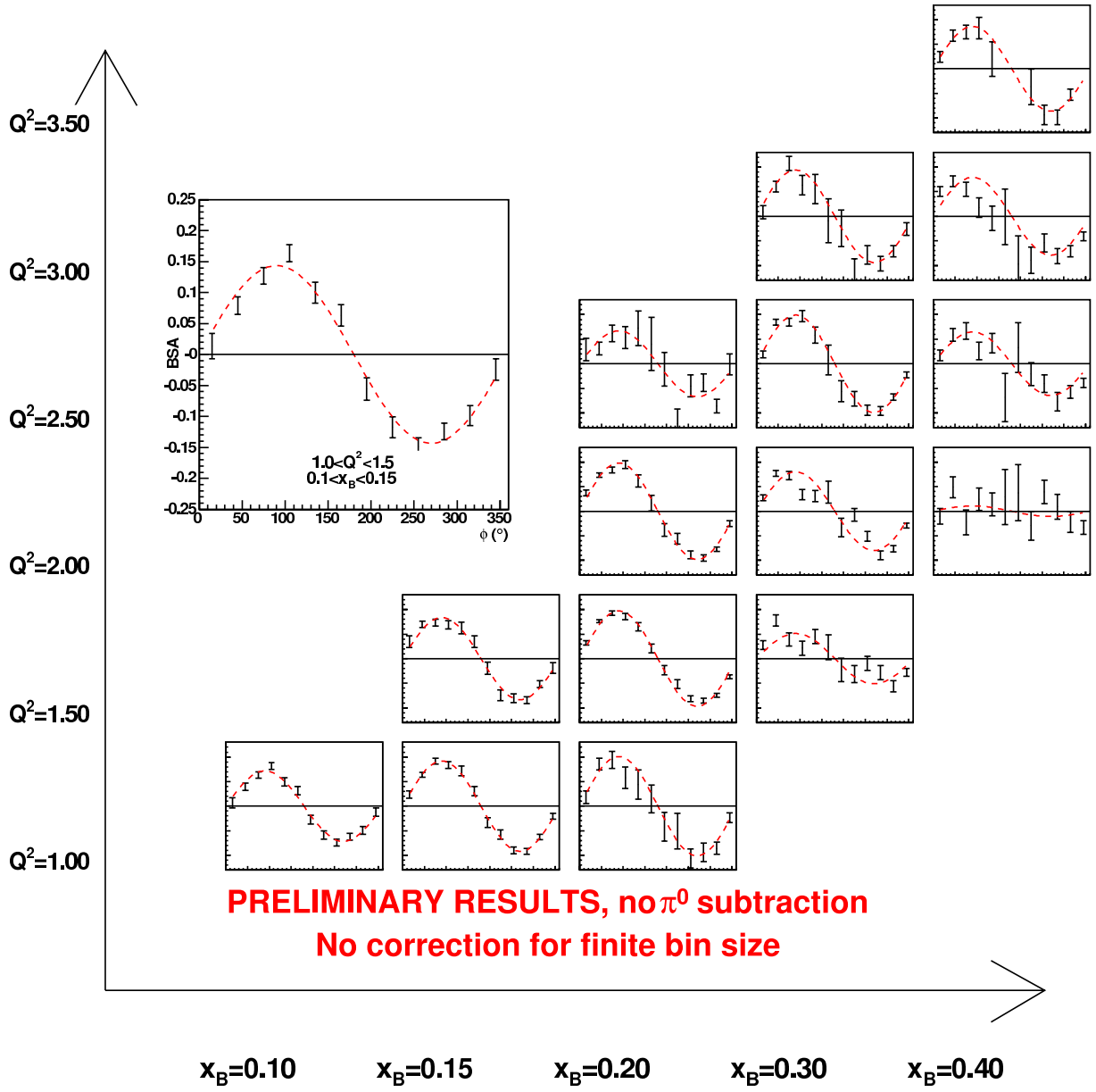

FIG. 8: E01-113 preliminary results: asymmetries for $ep \to ep\gamma$, not corrected for residual π^0 contamination and for finite bin size effects. Each plot is a distribution in φ (from 0 to 2π), for a given (Q^2, x_B) bin, integrated over all values of $-t < 0.8$ GeV^2 (this t-selection removes events at high x_B).

V. PROPOSED EXPERIMENTS AT 11 GEV

A. Experimental setup

The proposed experiments will use the standard CLAS12 setup. Please refer to [23] for detailed information. Note that the DVCS photon coverage can potentially be improved by either upgrading the Inner Calorimeter (IC) to larger angles, or by keeping it the same and bringing it closer to the target, at the expense of removing the High-threshold Čerenkov Counter.

The DVCS setup optimization will be performed once all mechanical issues of CLAS12 are worked out.

B. Super-conducting solenoid magnet as magnetic shield

The main source of background produced by a high-energy electron beam impinging upon a hydrogen target is due to interactions of the electron beam with the atomic electrons (Møller scattering). This rate is several orders of magnitude larger than the inelastic hadronic production rate.

The CLAS12 super-conducting solenoid magnet is designed with the goal of generating a homogeneous magnetic field of 5 T at the target location, parallel to the direction of the electron beam. It is also designed to keep Møller scattered electrons from reaching the CLAS12 detectors by guiding them to a shielding pipe made of heavy metal. The maximum luminosity at which CLAS12 can be operated is limited by the degree to which tracking chambers are shielded from the Møller electrons and secondary particles. This technique has been used successfully during the CLAS eg1, eg4 and e1-dvcs run periods, with the magnetic field provided by the 5 Tesla super-conducting Helmholtz magnet which was used with the CLAS polarized target, and by the 5 Tesla super-conducting solenoid which was used during E01-113 [8]. This arrangement resulted in significantly improved shielding than that provided by the mini-torus magnet which is the standard shielding configuration in CLAS being used for experiments with unpolarized targets.

Detailed GEANT-based simulations were performed to find the optimal shielding shape and position which provide the minimal background rates in IC in the CLAS12 configuration. The standard CLAS12 luminosity $\mathcal{L} = 10^{35}$ cm^{-2} sec^{-1} was assumed for these studies. The

simulations show that in these conditions the Møller electrons are confined to a cone with an opening angle of about 1.5 degree as seen from a 1.8 m distance to the production target. Møller electrons, which are the vastly dominating source of electro-magnetic background, will pass through the opening of the absorber and then through the central penetration in the lead-tungstate wall, and will be absorbed in the downstream shielding pipe as shown in Fig. 9.

Fig. 10 shows the estimated dose (in rad per hour) for inner calorimeter elements. Only the innermost two rings show signs of possible radiation damage. These studies are still under evaluation to optimize the experimental setup and the beam pipe shielding.

C. Longitudinally polarized target

The experiment to measure the longitudinal target-spin asymmetry proposed in this document requires use of a polarized solid state target, which is a part of the CLAS12 base equipment. The target will be polarized via the method of Dynamic Nuclear Polarization (DNP) which is a well established technique that has been used extensively in nuclear and particle physics experiments, including the ones performed in Hall B of Jefferson Lab. Dynamically polarized proton target systems consist of a hydrogenated compound containing paramagnetic centers, such as unpaired electrons, placed in a high magnetic field and cooled to low temperatures, with a $\mu B/kT$ ratio of the order of 5. In these conditions the free electron spins can approach polarization of 100%. The high polarization of unpaired electrons is then transferred dynamically to the nucleons by irradiating the target material at frequency near that of electron spin resonance. This technique typically achieves proton polarization of $80-90\%$. The nucleons in the target will be polarized longitudinally either parallel or anti-parallel to the electron beam direction.

The main systems required for realization of DNP are the superconducting magnet to provide a strong (5 T) field, a ^{4}He evaporation refrigerator to maintain target material at $\sim$ 1 K, a target insert which will house the target material and some additional instrumentation, a microwave system to transfer the polarization to nucleon spins and a Nuclear Magnetic Resonance (NMR) system to determine the state of polarization. In CLAS12 the polarizing magnetic field will be provided by the superconducting solenoid of the central detector. This will allow us to use the polarized target without introducing any obstructions on the paths

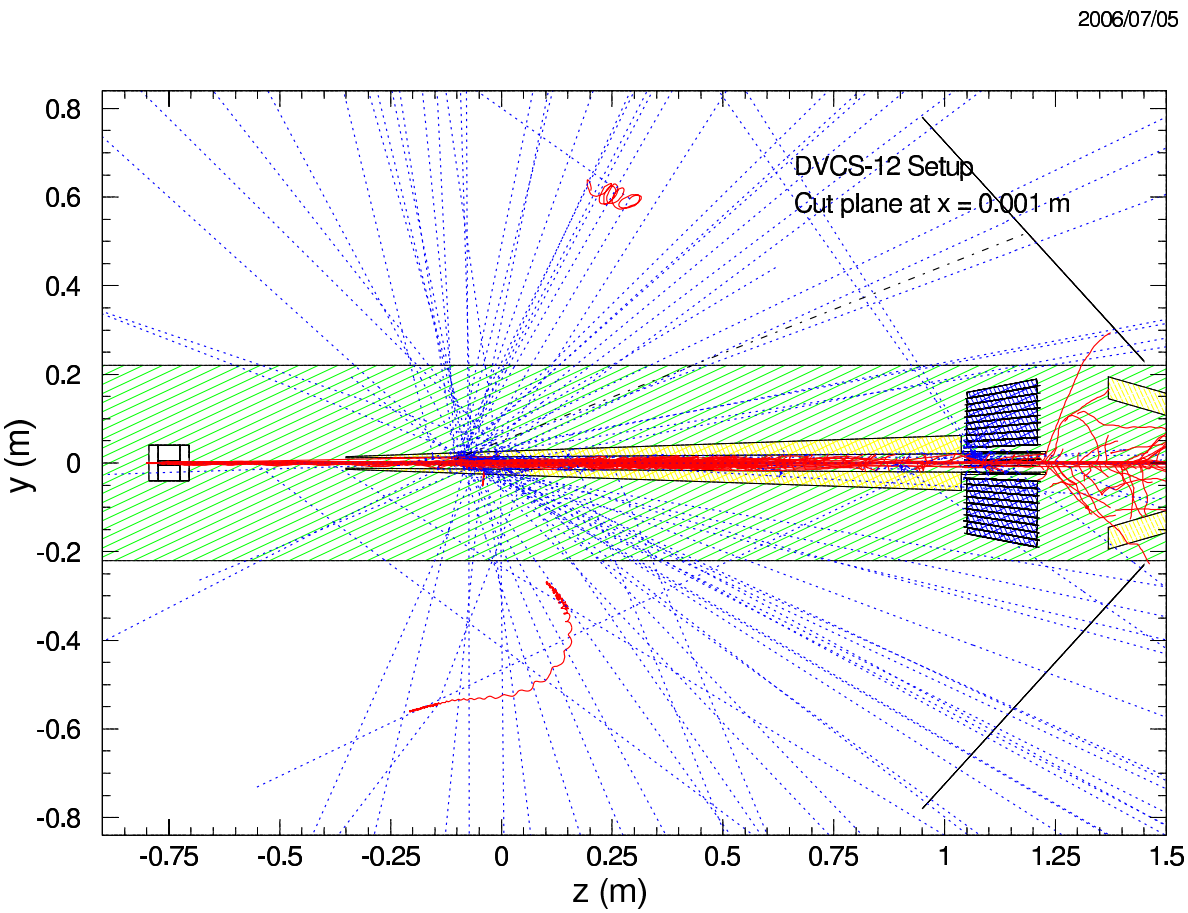

FIG. 9: Møller electrons from a GEANT-based simulation in the field generated by the CLAS12 solenoid magnet. The distance between the target and the face of IC is 180 cm. The beam pipe shielding covers angles up to 3 degrees. The beam pipe shielding is made out of tungsten which is the best shielding material for electrons and photons.

of the particles produced at the interaction point. The central detector will also be used in polarized target experiments, allowing for a wide coverage for particle detection, needed for measurements of multi-hadron final states.

The target cryostat will house the evaporation refrigerator, the target insert and some instrumentation necessary for the microwave and NMR operations. The cryostat needs to be designed to allow its operation in a warm bore magnetic field. A conceptual design of the target cryostat is shown in Fig 11. The main component of the cryostat is a ^{4}He evaporation refrigerator. The refrigerator is inserted horizontally through a pumping tube

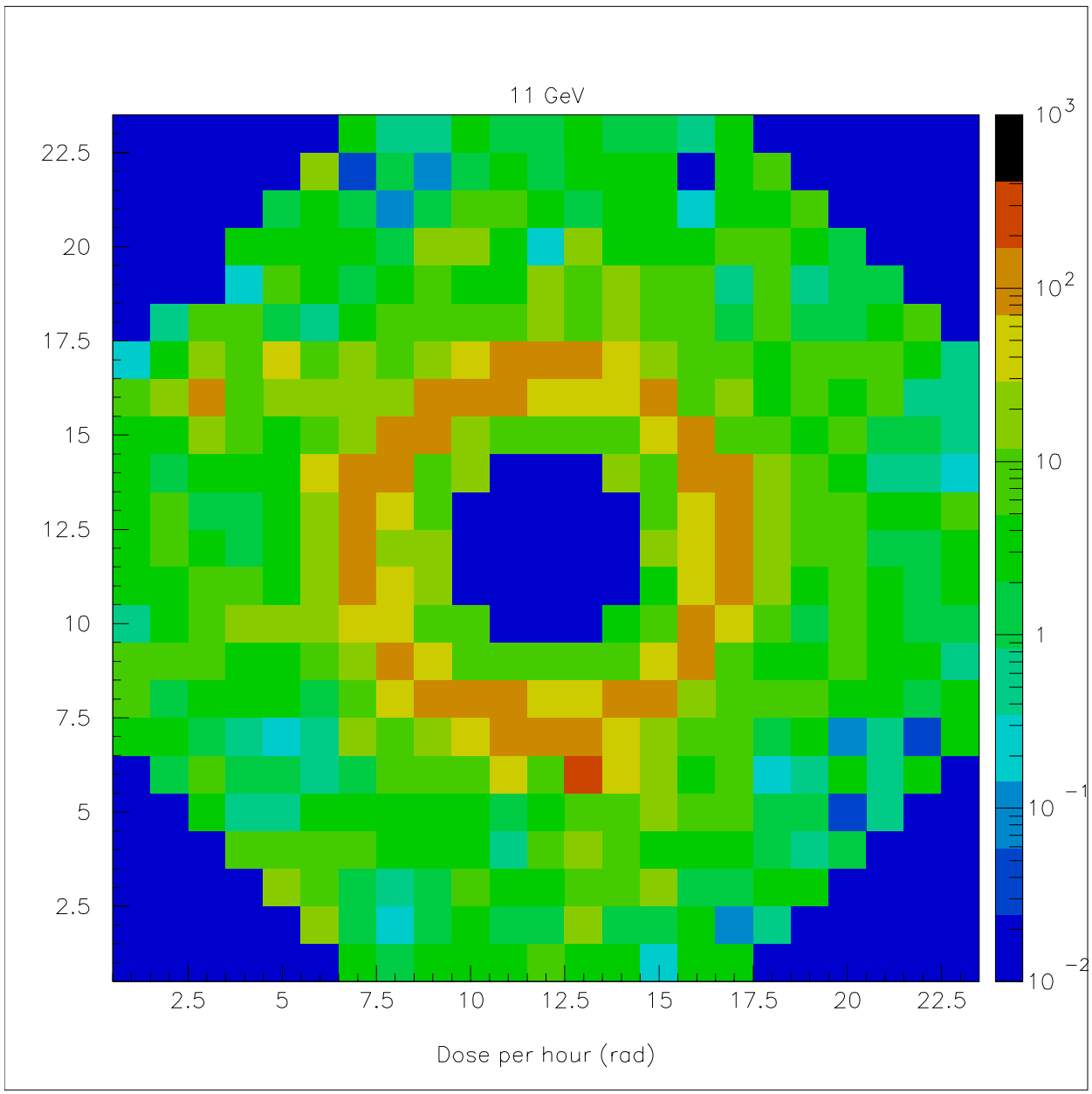

FIG. 10: Radiation dose, in rad per hour. Each square corresponds to an IC crystal.

between the pumps and the evaporation chamber. One important difference between this design and the previously used polarized target in Hall B is that the refrigerator will be residing along the beam line, so that the amount of materials in the way of the beam needs to be minimized. Liquid helium is supplied to the refrigerator through a transfer line from a dewar located outside of the detector. The liquid enters a copper separator pot, which

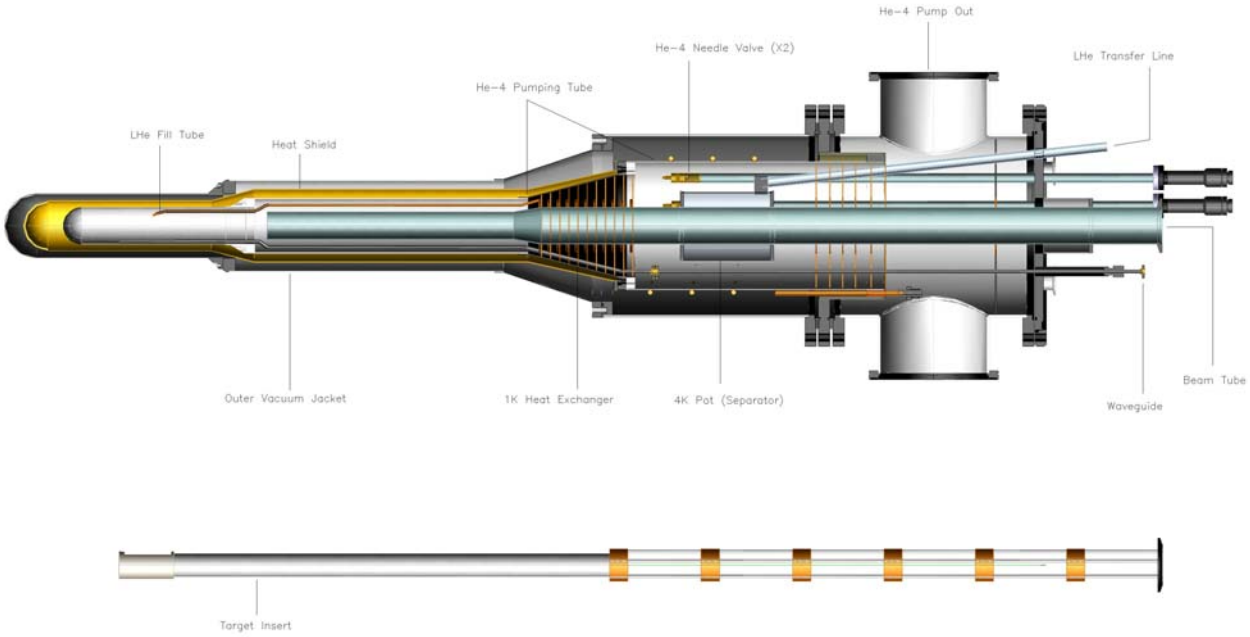

FIG. 11: A schematic drawing of the polarized solid target cryostat and the target insert for CLAS12.

will have a "doughnut"-like shape in order not to obstruct the beam path. In the separator, LHe is separated from the vapor by a sintered filter. The vapor is pumped away cooling the upper heat exchangers, and the liquid is used to cool the target material. Other detector components will also be installed in the magnet bore, so that the central tracker will surround the target, and impose constraints on the chamber dimensions. The minimum outer diameter in the present design of evaporation chamber is 10 cm. This volume will contain the outer vacuum space, heat shield and the evaporation chamber. The target material will be placed in a cell within a cup, with both containers made of hydrogen free plastic. The cup will be attached to a thin aluminum structure that can be inserted through the beam tube. The schematic of the insert is shown on the bottom of Fig. 11. The dimensions of the target cell will be determined by the size of region of field uniformity, and geometric constraints of the cryostat. The cup will have an opening on the top for the LHe fill, while the cell will have small holes so that the target material will be sitting in a "bath" of LHe, while also "showered" by LHe coming from the "run" valve. A flow of LHe in the cryostat will

TABLE II: Some parameters of the NH_3 targets

Target Diameter	up to 30 mm
Target Length	up to 100 mm
Density	0.917 g/cm^3
Dilution Factor	3/18
Packing Factor	~ 0.62

be maintained by a series of pumps located outside of the cryostat. The entrance and exit windows of the target cell and cup could be made out of thin aluminum or capton foils. The microwave radiation needed to polarize the target will be guided through a designated waveguide inserted through the upstream entrance window of the cryostat. The guide will have a slit directly underneath the target cup, providing continuous microwave radiation directed at the target beads in the target cell. With this arrangement, the target cup will act as a resonating cavity.

Ammonia will be used as target material with the electron beam and CLAS12. This target offers high polarization, good resistance to radiation damage, and a relatively high ratio of polarizable nucleons per total number of nucleons. Ammonia can accumulate charge of $\sim 10^{15}$ electrons/cm^2 before showing signs of deterioration. Accumulated radiation damage can be mostly restored through the annealing process, in which target material is heated to temperatures of $80 - 90$ K for short period of time. Some parameters of frozen ammonia are listed in Table II.

In order to determine the effective dilution factor D_{eff}, it will be necessary to collect data on the unpolarized material. A thin carbon target could be placed downstream in the same target cup for this purpose.

The target polarization will be monitored during the run via the NMR system in the field of the solenoid magnet. The calibration of the proton NMR can be done by measurements of polarization in thermal equilibrium, taken with the polarizing magnet. Typical NMR signals for a polarized proton target [24] are shown in Fig. 12.

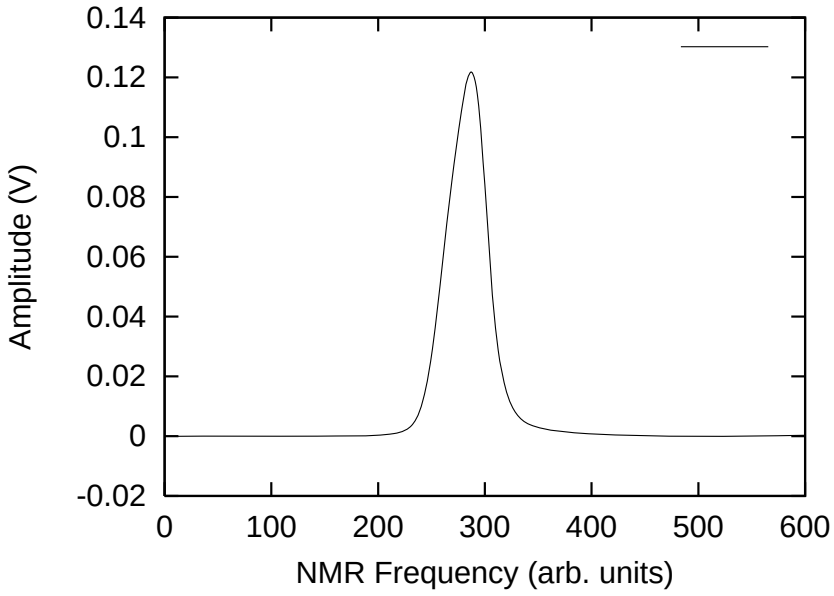

FIG. 12: NMR signals for polarized NH_3.

D. Event reconstruction and identification

The event identification in CLAS12 will be accomplished in a similar way to E01-113 [8], using charged particle tracking in the torus and solenoid magnetic fields and time-of-flight systems in both forward and central detectors. Electrons will be separated from pions using the high-threshold Čerenkov counter and the forward electromagnetic calorimeter (EC). Protons will be identified using time-of-flight (SC/CTOF) and path length plus measured momentum (DC/central tracker). Photons will be detected in both the inner calorimeter (IC) and EC. Only events with $W > 2$ GeV will be selected to avoid significant contributions from excitations of nucleon resonances.

One of the main problems encountered in the previous analyses of DVCS data is the background from π^0 production events, where π^0 decays into two photons and only one of them is detected. The relative amount of the π^0 contamination is expected to be small at lower values of $|t|$, and to increase with $|t|$.

In order to select single photon production events we will detect all three particles in the final state, and require that there are no extra photons in the detector. Kinematical consistency cuts, such as missing energy/momentum cuts will be applied, similar to those used in E01-113 and described in Section IV. To estimate the effectiveness of these methods

at 12 GeV beam energy a large number of single photon and π^0 events were simulated. The output of the event generator were processed with the *FastMC* program [25], which simulates the response of the CLAS12 detector. A cut on missing energy over measured photon energy $E_{miss} < 0.1\sqrt{E_\gamma}$, shown in Fig. 13, will allow for very few pion events in the data set without causing a large reduction of $ep \to ep\gamma$ events. Additionally, selecting only events within 0.6° and 2° cone around the expected direction of the photon, detected in IC or EC respectively, (see Fig. 13), will further reduce the single π^0 background. Note that although these energy and angle cuts are somewhat tighter than in Fig. 7, the tracking reconstruction can still be improved in E01-113 to allow for tighter kinematical constraints. Using Monte-Carlo simulations we estimated that these two cuts will reduce the π^0 background on average by a factor of 10, while the number of the photon production events will decrease by approximately 20%. The simulations also indicate that after these cuts the pion contamination in some bins at $-t = 0.7$ can be up to 50% of the total number of events, while at small values of $-t = 0.1$ GeV^2 it is of the order of 1%. Note that even if the π^0 electroproduction did not produce asymmetries, the measured values would be diluted by the background events.

The strategy for accounting for the contribution of the remaining π^0 events into the spin asymmetries is to evaluate the amount of π^0 contamination, and subtract their contribution to the measured asymmetry. In the first step the π^0 yields and spin asymmetries will be measured using $\pi^0 \to \gamma\gamma$ decays, where both photons are detected in CLAS12. In the next step, using Monte-Carlo simulations to calculate the acceptance ratio between 1-γ-detected and 2-γ-detected π^0 events, we can infer the number of π^0 production events in the (e, p, γ) data sample. This method is being used in the data analysis of E01-113 Hall-B experiment. A similar technique was used with simulated events at 11 GeV electron beam energy, and the results are illustrated in Fig. 14. The (Q^2, x_B, $-t$) bin shown on the right is one of the worst cases of π^0 contaminations. The plot on the left represents a typical case. The red circles show the target-spin asymmetries for pure DVCS/Bethe-Heitler event sample from the model [11] incorporated in the event generator [26] which was used in this study. After mixing in 26% of single π^0 electroproduction events the asymmetries are distorted, shown with green triangles. After accounting for these events by evaluating the single photon asymmetry in the π^0 data sample, and subtracting it from the "measured" asymmetry, we obtain the blue squares - the corrected values of the asymmetry, which are close to the

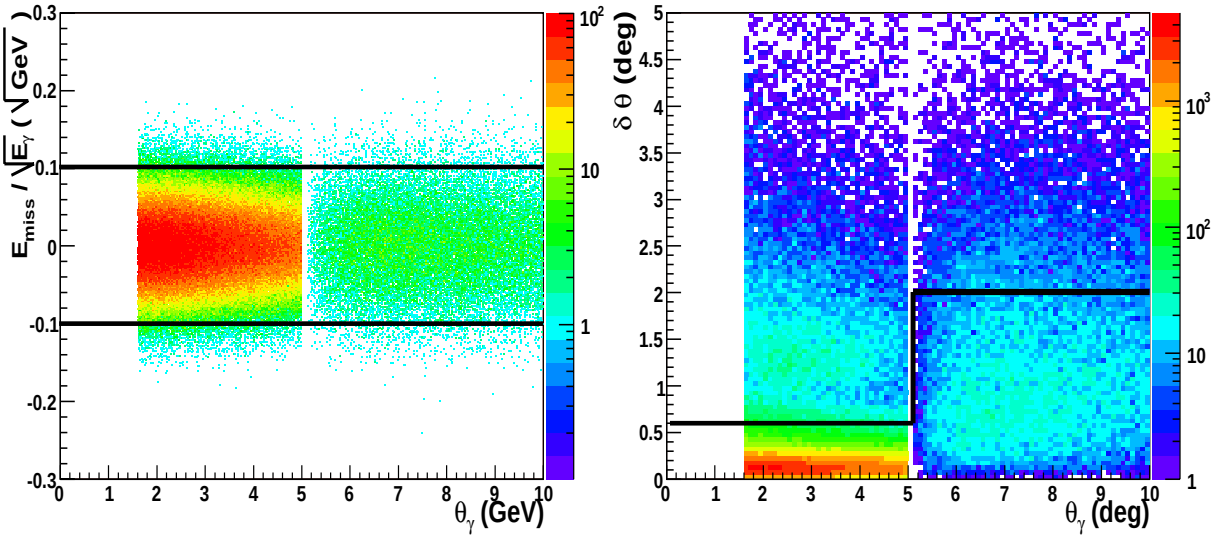

FIG. 13: Missing energy versus photon angle in the laboratory frame (left), and the angle between expected difference of photon and the angle of the detected photons versus photon angle (right). In each plot, the tow loci correspond to IC and EC polar angle coverage. The black lines show the cuts applied to reduce pion contamination. Only DVCS/Bethe-Heitler simulated events, processed with *FastMC* detector simulation program, are included in this plots.

original single photon asymmetry. The difference between the blue squares and the red circles indicate the expected uncertainties from the described procedure. For a typical case represented in the left plot on Fig. 14 the corrected and the pure DVCS asymmetries are virtually indistinguishable.

E. Acceptance

The CLAS12 acceptance for $ep \to ep\gamma$ reaction was estimated using Monte-Carlo simulations. The event generator [26] used to estimate the acceptance for the DVCS experiment is based on the GPD formalism described in Ref. [11]. Single photon electroproduction events at the beam energy 11 GeV were simulated in the $2 < Q^2 < 10$ GeV^2 range. These events were processed with the *FastMC* computer program [25] to simulate the CLAS12 detector response. This program represents a set of cuts in the coordinate and momentum space to represent the areas of the detector acceptance where the detection efficiency is expected to be close to unity. These cuts are combined with parameterizations of the detector response from various components of CLAS12. The efficiency of the active detector volumes

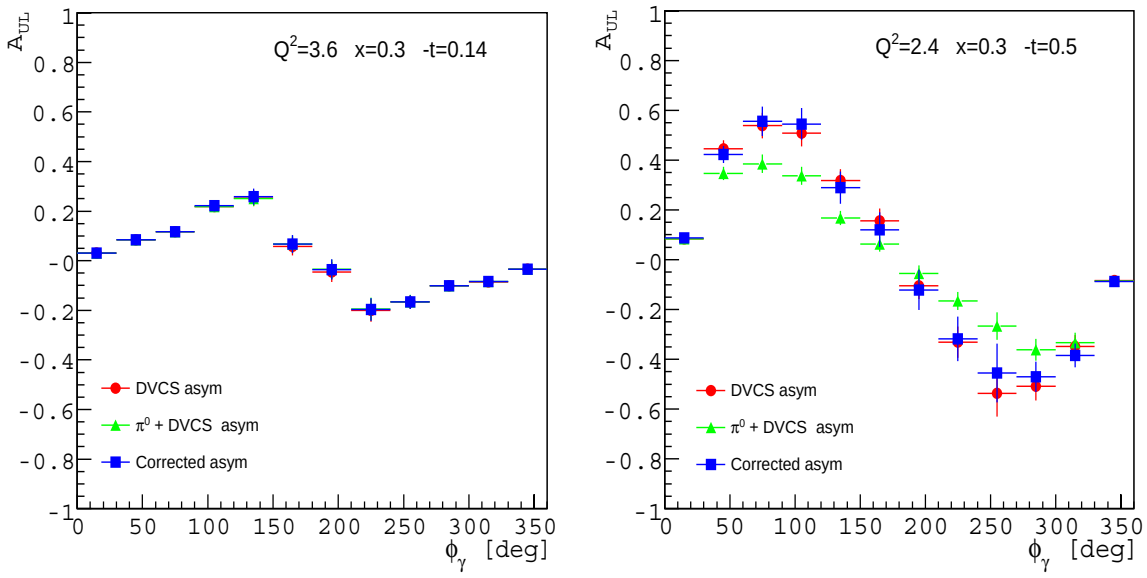

FIG. 14: Simulated target spin asymmetries for pure single photon data sample (red circles), data sample contaminated with π^0 events (green triangles), and asymmetries after subtracting π^0 contribution (blue squares). Error bars on these plot show the statistical uncertainties defined by the number of simulated events. The right plot represents one of the cases with the largest discrepancies between the pure DVCS and corrected target spin asymmetries. A typical case is presented on the left plot.

is considered to be one. The φ-dependences of the acceptance at fixed values of Q^2, x_B for $-t = 0.35$ GeV^2 is shown in Fig. 15. It is evident that CLAS12, due to its large kinematic coverage, is well suited for conducting DVCS experiments. Nevertheless, the same studies show that the CLAS12 acceptance for DVCS can still be improved, especially at high x_B and Q^2.

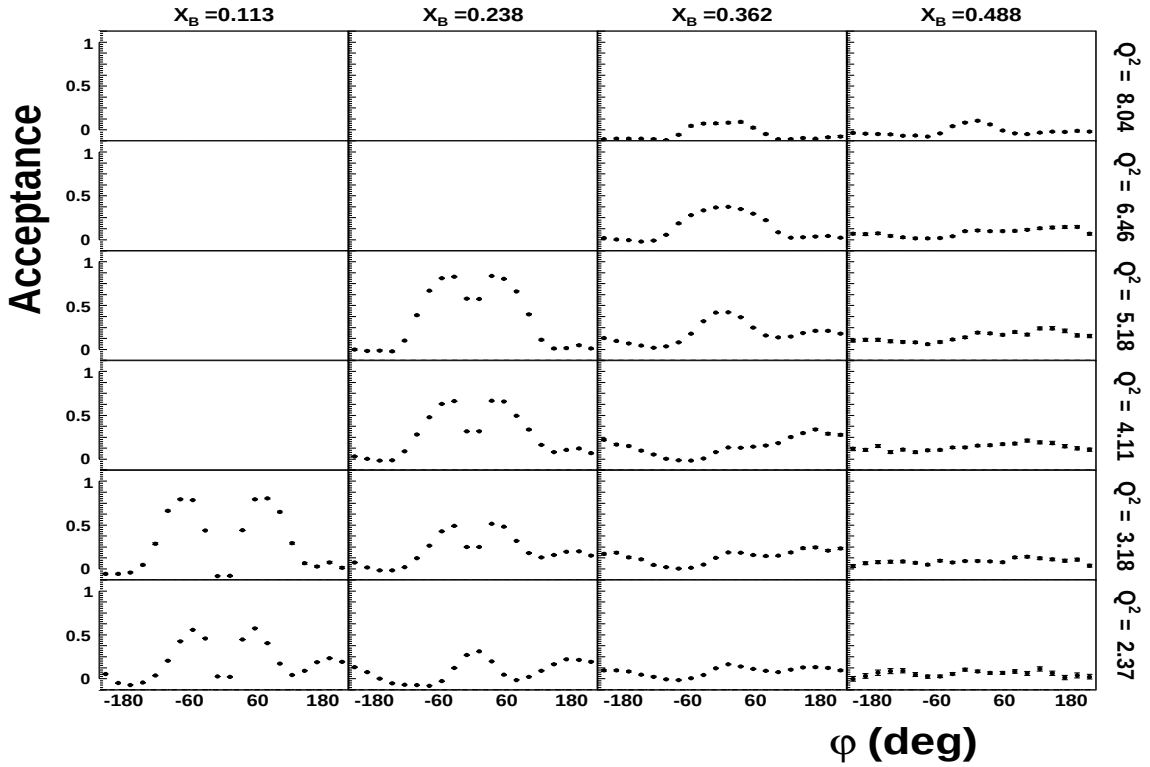

FIG. 15: Projected acceptances for the DVCS/BH events versus φ for different Q^2 and x_B values at $-t = 0.35$ GeV^2.

VI. COUNTING RATE ESTIMATES FOR 11 GEV

A. Beam spin asymmetries

1. *Counting rate estimates*

The number of DVCS events expected in a certain bin in x_B, Q^2, t, φ and azimuthal electron angle ϕ_e is given by:

$$N = \mathcal{L} \cdot time \cdot \sigma \cdot (\Delta Q^2 \cdot \Delta x_B) \cdot \Delta t \cdot \Delta\varphi \cdot (\Delta\phi_e)_{eff}/2\pi \,. \tag{27}$$

CLAS12 is expected to run at a luminosity of $\mathcal{L} = 10^{35}$ cm^{-2}s^{-1}. The acceptance in (x_B, Q^2) might not always reduce to a simple rectangle depending on the considered bin, because of the limitation in the electron scattering angles, maximum energy and the requirement $W > 2$ GeV to exclude resonances from this study. $(\Delta\phi_e)$ corresponds to the electron azimuthal acceptance, which is not 2π, especially at low electron scattering angle. Models used to estimate the cross-section always give a ϕ_e-integrated result, hence the $(\Delta\phi_e)_{eff}/2\pi$

factor. Finally, the model used for the photon electroproduction cross section σ is a modified version of the VGG model [27], with a Regge-inspired ξ-dependence. The acceptance ranges from 0.1 to 0.5 depending on which bin is considered. As usual CLAS12 itself has a strong azimuthal angle dependence which translates directly in modulations in φ. Finally, the counting rates have been estimated for **80 days of 85%-polarized beam on target**.

Figure 16 shows the binning in (x_B, Q^2) used to present the pseudo data generated using the CLAS12 version of FastMC [25]. This binning is arbitrary and as is clearly seen on the figure, does not take into account very low-x_B and high-x_B/high-Q^2 data, which is also of interest. Figure 17 shows the asymmetry for the proposed (x_B, Q^2, t) bins. In addition there are 20 bins in φ and the results are integrated over ϕ_e. Note that $-t$ as high as 2 GeV^2 were generated, and high t are mostly contained in the last t bin which is therefore quite wide. The error bars are purely statistical. The $\sin\varphi$ harmonic extracted from this data will have a statistical error from 1% at low x_B and "low" Q^2 (lower left corner of the plot) up to 10% at the highest x_B and t (right section of the plot), which are of the same order of the planned systematic uncertainty of about 5% average.

Figure 18 is a detail of particular bins in our pseudo data sample, showing the statistical accuracy of the planned measurement along with different scenarios for a GPD model. The level of precision this proposal plans to achieve will be decisive for putting strong contraints on GPD parametrizations.

2. Systematic errors

Since the main goal of this program is the measurement of relative asymmetries, most sources of experimental uncertainties such as acceptance, efficiencies, dead time, cancel in the ratio to first order. However, due to the strong φ modulation of the CLAS12 acceptance, a small systematic error will arise from the acceptance. This effect is not so dramatic when one is able to make enough φ bins in the data, which will be the case in the proposed experiments (at least 20 bins in φ). We expect the systematic error coming from this φ acceptance modulation to be of the order 3% in the worst case.

A typical source of systematic error arises from the π^0 contamination corrections. In order to estimate the uncertainty in the BSA, a large number of single photon and π^0 events have been mixed with a known weight and used in the Monte-Carlo. The method explained

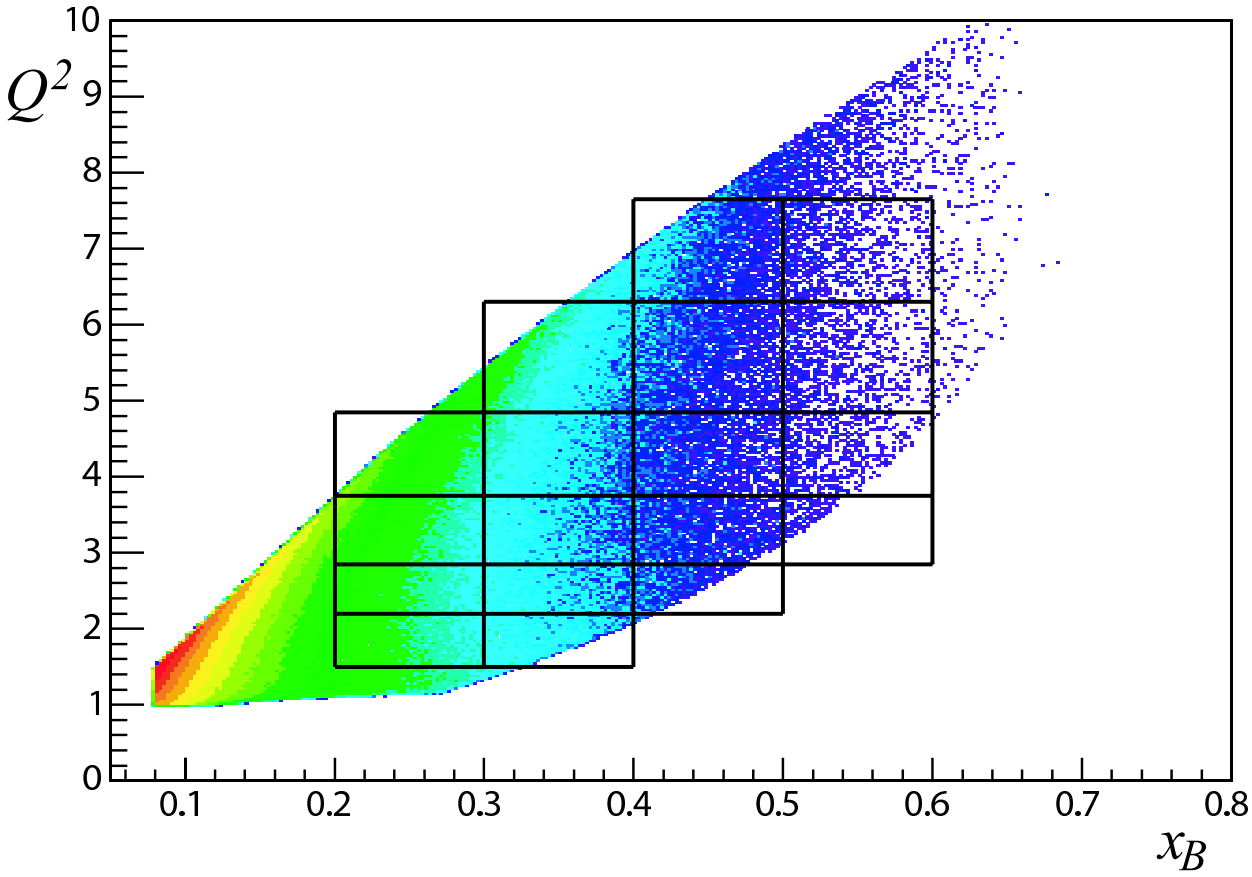

FIG. 16: Kinematical domain in (x_B, Q^2) of 11 GeV running with CLAS, with the conditions that $W > 2$ GeV to exclude resonance region. Also shown is the binning in x_B and Q^2 used to evaluate counting rates in this section.

in Section V D was used to correct the asymmetry from the systematic π^0 background. Whereas at low-t, the π^0 contamination is expected small, high-t bins have much more π^0 making it more difficult to subtract them reliably. It has been estimated that the π^0 correction procedure induces a systematic error ranging from 1% to 5%.

Beam polarization enters directly as a correction to the BSA and it is estimated to be the source of a 2% systematic error on our observable.

Radiative corrections are known to produce effects on the BSA of 5% at most at Jefferson Lab kinematics [28], yielding systematic uncertainties of the order 0.5% only, to the best of our current knowledge.

Overall, the systematic uncertainties on the BSA will range from 4% to 6% depending on the bin, with roughly half being normalization errors and half point-to-point errors.

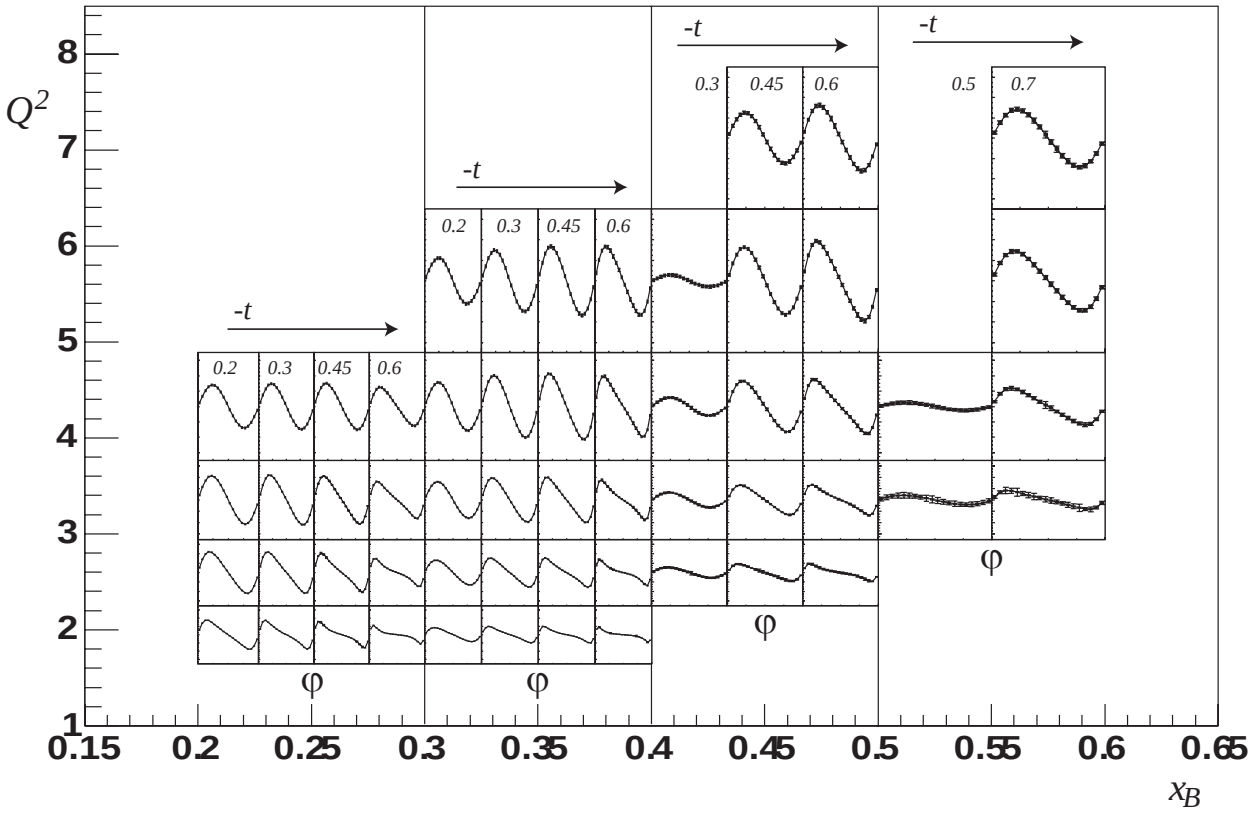

FIG. 17: Kinematical coverage of the beam spin asymmetry as a function of (x_B, Q^2, t). The outer horizontal scale corresponds to the x_B range, divided into 4 bins. The outer vertical scale represents the Q^2 range. Each individual histogram is the BSA (plotted between -0.7 and 0.7) as a function of φ (between 0 and 2π) for a given t-bin. The average value of $-t$ in the bin is shown in the upper part of each histogram. Only statistical errors are show. Relative statistical accuracy on the $\sin\varphi$ harmonic extends from 1% in the lower left section of this figure to 10% in the upper right section assuming 80 days of running at 10^{35} cm^{-2}s^{-1} luminosity.

Cross-section measurements is a secondary goal of this experiment, and will be achieved with reasonable systematic accuracy, around 10%. A summary of systematic sources and associated relative uncertainty can be seen in Table III.

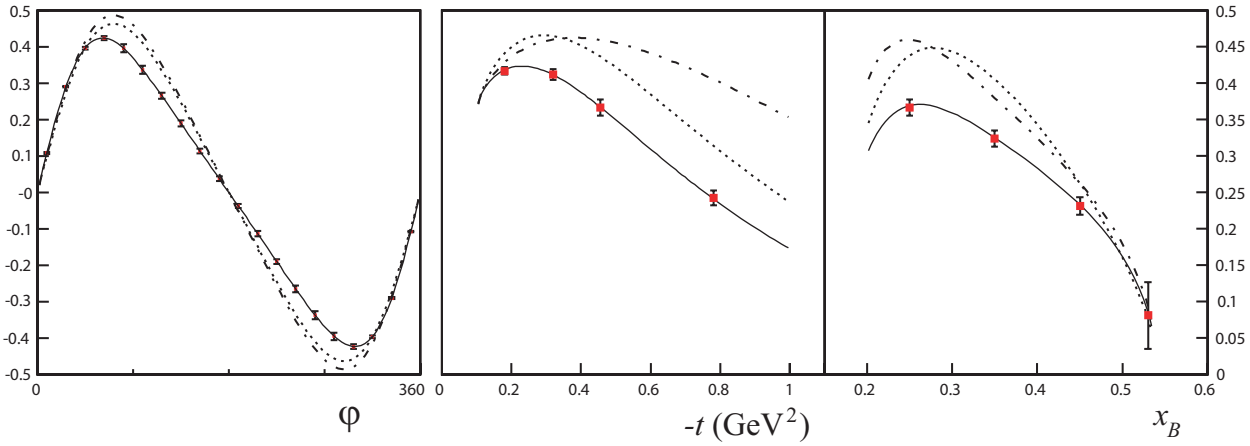

FIG. 18: On all figures: points in red represent data with statistical error bars. Lines are models with different input parameters, none of which includes twist-3 contributions: The full line is a model with a Regge-type t-dependence and D-term. The dotted line includes the Regge-type t-dependence but has no D-term. The dash-dotted line has the D-term but the t dependence only comes from form factors. Left figure: Beam spin asymmetry as a function of φ for $< x_B >= 0.2$, $< Q^2 >= 3.3$ GeV^2 and $< -t >= 0.45$ GeV^2. Middle figure: BSA as a function of $-t$ for $< x_B >= 0.2$, $< Q^2 >= 3.3$ GeV^2 and $\varphi = 90°$. Right figure: BSA as a function of x_B for $t = 0.45$ GeV^2, $< Q^2 >= 3.3$ GeV^2 and $\varphi = 90°$.

B. Target spin asymmetries

1. *Measurement*

The desired final state in this experiment is (e, p, γ) with no additional charged tracks or photons detected in CLAS12. The missing mass technique with the detection of the electron and one proton does not work in this case due to inadequate $\pi^0 - \gamma$ separation in the missing mass spectrum. Therefore all three particles in the final state will have to be detected. In order to reduce the contributions from nucleon resonances a $W > 2$ GeV cut will be applied. The details of the single photon production event selection procedure is described in Section V D.

The experimental target spin asymmetry is calculated as a ratio:

$$A_{UL} \equiv \frac{1}{P_T F} \frac{N^+ - N^-}{N^+ + N^-}, \tag{28}$$

where N^+ and N^- are the numbers of counts in each bin for positive and negative polar-

Source of error	BSA	$\Delta\sigma$	σ
Beam polarization P_e	2%	2%	-
π^0 contamination	1-5%	1-5%	3-8%
Acceptance	3%	8%	8%
Radiative corrections	1%	3%	3%
Luminosity	-	2%	2%
Total	4-7%	9-10%	9-12%

TABLE III: Expected systematic errors for beam helicity asymmetries, cross-section difference and sum.

ization of the target, P_T and F are the target polarization and dilution factor for the event sample, respectively. The effective polarization of the target will be extracted by measuring the double spin asymmetry from elastic electron scattering. The full simulations of this method with CLAS12 detector yield uncertainty on $P_e \cdot P_T$ product of about 1%. Therefore, the uncertainty on the target polarization will be dominated by the precision of the Møller polarimeter, which is estimated to be about 2%.

2. Background

One of the main sources of the background events is the single photon production from the unpolarized nuclei in the target material. Such events will not produce target spin asymmetry, and therefore will only reduce the measured asymmetry. This kind of background can be reduced using missing energy cuts, assuming an electron scattering process from a free proton. Due to Fermi-motion in the nuclei, the distribution of the components of the missing momentum are smeared around zero, and such a cut will significantly reduce the background from the nuclear target. A similar technique has been successfully used in the analysis of CLAS data [9], where a 2° cut was applied to the difference between expected angle for the photon and the measured photon. Data taken with a solid ^{12}C target will allow us to determine the the dilution factor using a similar technique described in Ref. [9].

Accidental two-gamma coincidences and radiative processes, such as $ep \to e\gamma N^* \to e\gamma p\gamma$, can also produce background. But the rate for the former is expected to be low due to good time resolution and 100% duty factor of the CEBAF beam. The latter process is suppressed by two orders of magnitude with respect to the hadronic processes.

3. Statistical accuracy

To estimate the statistical accuracy of the proposed experiment DVCS/Beth-Heitler events were simulated using a generator [26] based on Ref. [11], and were processed with *FastMC* computer program [25]. The simulated data sample was binned in Q^2, x_B, $-t$ and φ. The event yield in each bin can be found using Eq. (27). In order to calculate the number of events in each bin we assumed $\mathcal{L} = 2 \times 10^{35}$ cm^{-2} sec^{-1} instantaneous luminosity and total number of 100 days of beam time on polarized ammonia. The factor of 2 increase for luminosity with respect to unpolarized runs can be achieved considering that nuclear targets, like NH_3, contain half the Møller scattering targets compared to liquid hydrogen. The target polarization in this estimate was assumed to be $\sim 80\%$. The distribution of the number of events detected in CLAS12 for different Q^2 and x_B bins at $-t = 0.35$ GeV^2 is presented in Fig. 19. The bin occupancy is plotted in logarithmic scale to suppress the sharp peak at $\varphi = 0^\circ$ for DVCS/Bethe-Heitler events. A plot showing target spin asymmetries versus φ with the expected statistical errors is presented in Fig. 20. The bin sizes in these plots have not been optimized, they will be chosen to best match the statistical and systematic uncertainties of the data. The values for the target asymmetries are calculated using a model which reasonably describes the existing CLAS data [28]. Clearly the statistical errors are small at small x_B, and the expected relative statistical uncertainty for $A_{UL}^{\sin\varphi}$ is $\frac{\sigma_A}{A} \sim 2\%$. The statistical errors become larger in the high x_B region $x_b > 0.4$, and the expected relative uncertainty for extracted $A_{UL}^{\sin\varphi}$ is $\frac{\sigma_A}{A} \sim 10\%$. Sample plots showing the sensitivity of the target-beam asymmetry measurement to $\widetilde{H}$ is presented in Fig. 21. The φ dependence of the target spin asymmetry at $Q^2 = 4.1$ GeV^2, $x_B = 0.36$ and $-t = 0.52$ GeV^2 is shown in Fig. 21 a. The black points show the values from Ref. [28] using CTEQ6 PDFs [29] with the projected statistical errors for the proposed measurement. The red solid curve is obtained using MRST02 PDFs [30] with $E = \widetilde{E} = 0$, and for the blue dashed curve $\widetilde{H}$ is set to zero as well. Figs. 21 b and c show the $-t$ and x_B dependences of the $\sin\varphi$ moments extracted by

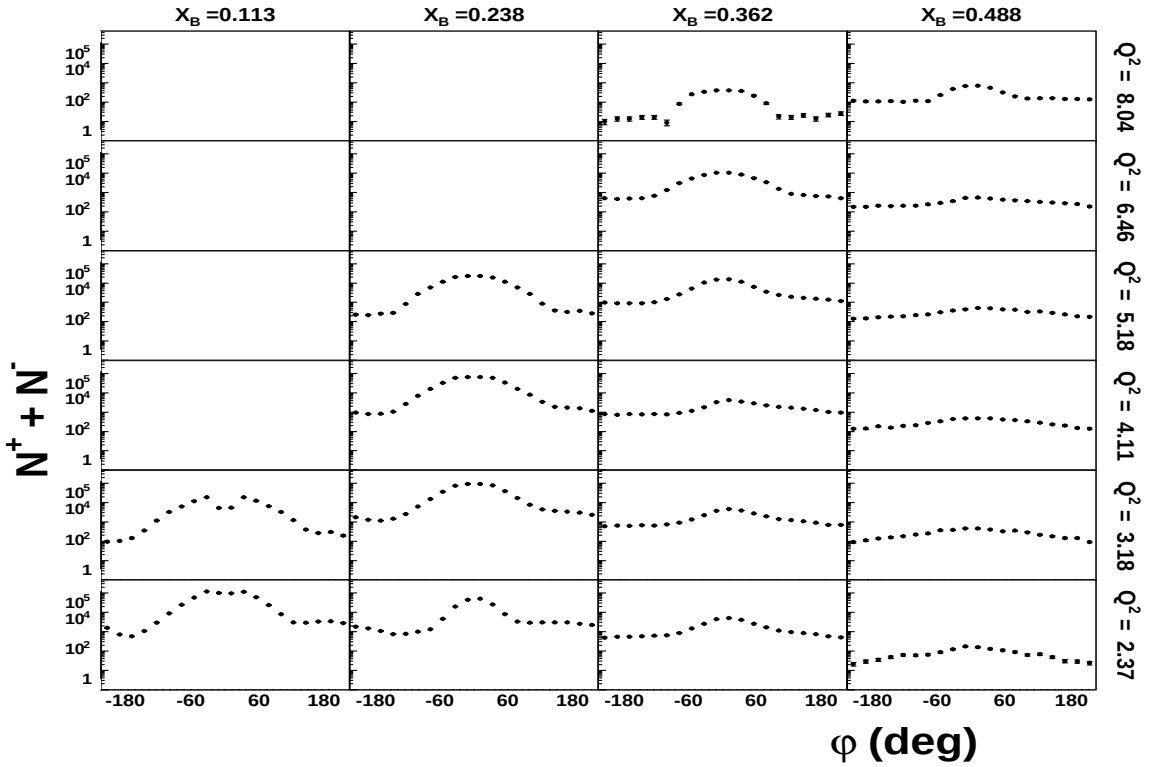

FIG. 19: Projected number of events versus φ for different Q^2 and x_B values at $-t = 0.35$ GeV^2. The error bars represent the statistical uncertainties.

fitting the φ dependent histograms for target beam asymmetry with a function of the form $f(\varphi) = \alpha \sin\varphi + \beta \sin 2\varphi + \gamma$. The error bars in these plots are defined by the statistical uncertainties in the corresponding φ dependent histograms. At the lower values of $-t$ and x_B the errors will be dominated by the systematics, while at higher $-t$ and x_B the statistical and systematic errors are expected to be of the same magnitude. The difference between the red solid curve and blue dashed curve is due to $\widetilde{H}$. Therefore these data along with beam-spin asymmetries and cross section differences will allow for extraction of the $\widetilde{H}$ with high accuracy using a combined fitting procedure.

4. Other systematic uncertainties

One of the main advantages of measuring asymmetries is that most of the experimental systematic uncertainties in the first order cancel in the ratios. But the uncertainties in the knowledge of certain quantities, such as backgrounds or the target polarization, still need to be accounted for. The main background to the single photon production on the polarized

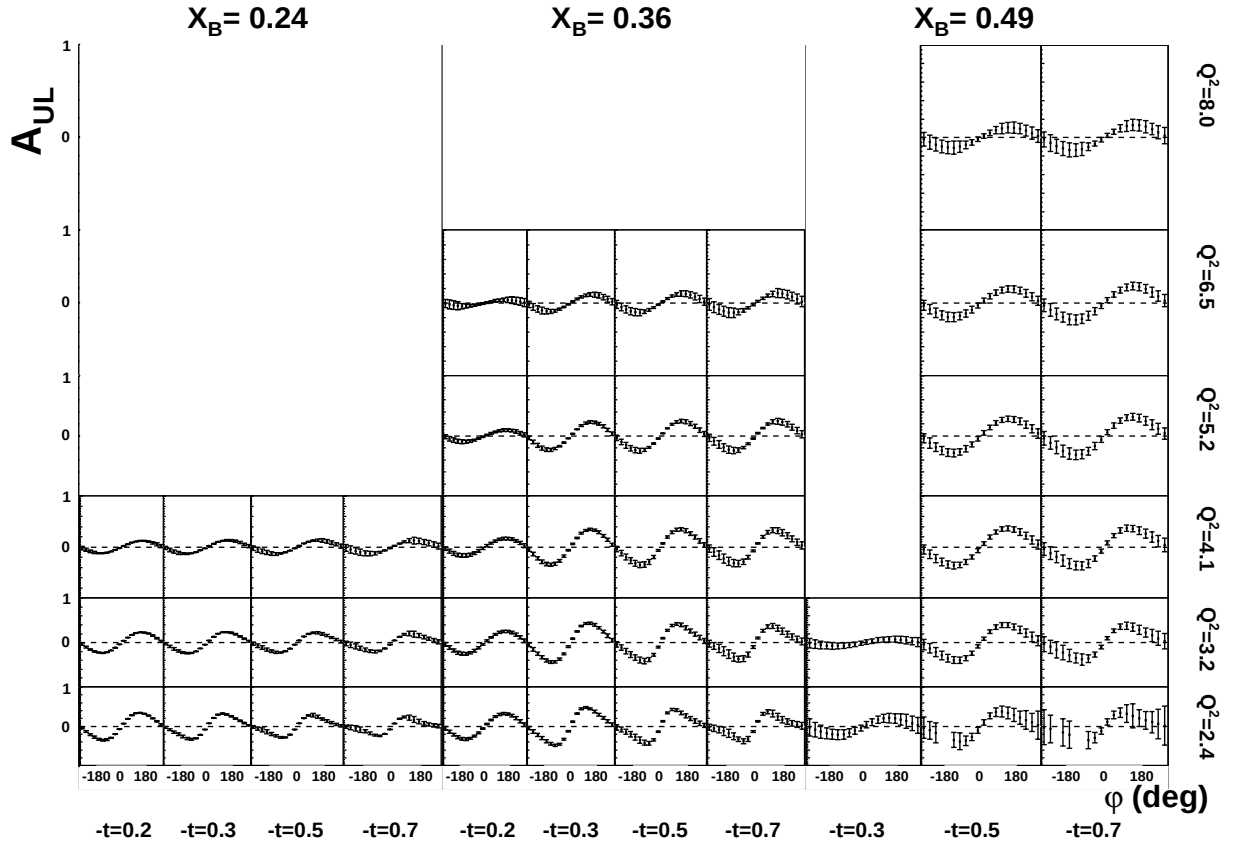

FIG. 20: Target spin asymmetry versus φ for different Q^2 and x_B and $-t$ values.The error bars represent the projected statistical uncertainties for the target spin asymmetry using the Monte-Carlo simulation. The asymmetry values are from Ref. [28].

proton is the photon production from the nuclear material in the target. These events will dilute the target asymmetry and will be removed from the data set with a procedure described in the previous sections. The remaining relative uncertainty for the asymmetries in this procedure is estimated to be $\sim 4\%$.

Another source of background for this experiment is expected to be from π^0 contamination. In order to estimate the uncertainty in the TSA, a large number of single photon and single π^0 electroproduction events were simulated and mixed together with a ratio obtained from Ref. [26]. The asymmetry from the single π^0 production was then subtracted from the combined asymmetry as described in Section V D. The results for the subtracted asymmetries were compared to the asymmetries for pure photon events to estimate the uncertainties coming from the π^0 production channel. The relative systematic errors due to single π^0 contamination are estimated to be varying between 1% and 5% depending on the

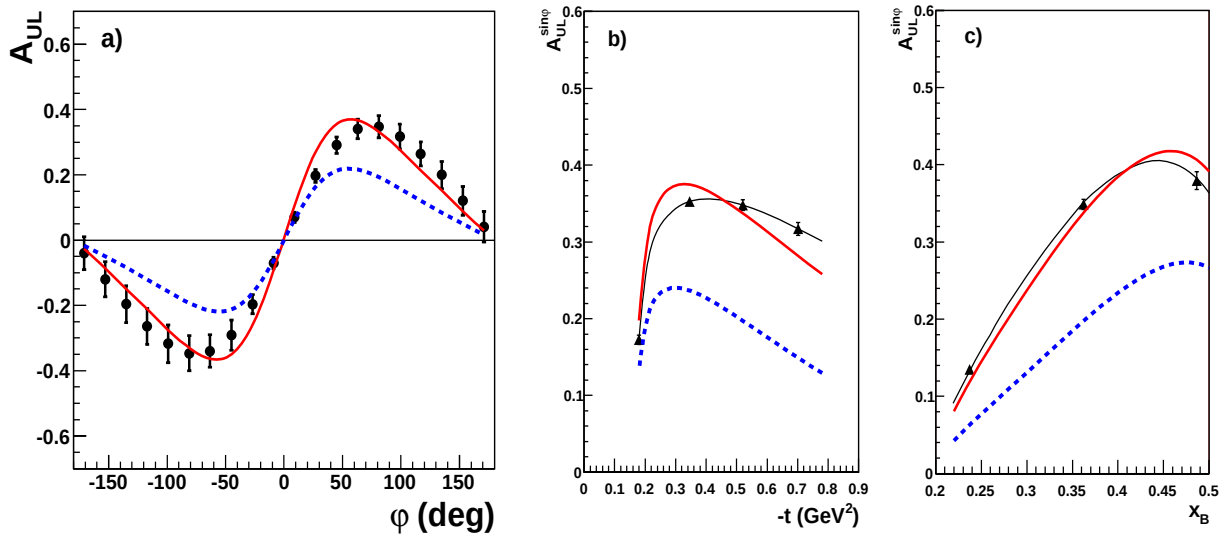

FIG. 21: Target spin asymmetry versus φ for $Q^2 = 4.1$ GeV^2, $x_B = 0.36$ and $-t = 0.52$ GeV^2 (a). The black points show the values from [28] using CTEQ6 PDFs with the estimated errors from the proposed measurement. The red solid curve is using MRST02 PDFs with $E = \widetilde{E} = 0$, and for the blue dashed curve is $\widetilde{H}$ is also set to zero. $\sin\varphi$ moments of the target spin asymmetry versus $-t$ at $Q^2 = 4.1$ GeV^2 and $x_B = 0.36$ (b), and versus x_B at $Q^2 = 4.1$ GeV^2 and $-t = 0.52$ GeV^2 (c). The projected error bars represent the statistical uncertainties only.

kinematics.

We summarize various contributions to the relative systematic uncertainty in Table IV. The total systematic uncertainty for the single photon electroproduction target spin asymmetry is estimated to be 6% to 8%, comparable with the projected statistical errors.

5. *Summary for target asymmetry experiment*

We propose to study Generalized Parton Distributions via measurements of Deeply Virtual Compton Scattering above the resonance region and for $Q^2 > 2$ GeV^2, using the upgraded CEBAF electron beam with an energy of 11 GeV incident on a longitudinally polarized target, and the basic components of the upgraded CLAS12 detector. Our projections show that we can achieve high statistical accuracy using 120 days at $\mathcal{L} = 2\times10^{35}$ cm^{-2} sec^{-1} instantaneous luminosity. The beam time needed for various activities is presented in Table V. The contributions of the DVCS process will be identified via the interference with the Bethe-Heitler process by measuring target spin asymmetry. The main systematic uncer-

TABLE IV: Expected relative systematic uncertainties for target spin asymmetries.

Source	Systematic Uncertainty
Nuclear material	4%
P_T determination	3%
π^0 contaminations	1% - 5%
Acceptance	3%
Accidentals	1%
Radiative corrections	1%
Total	6% - 8%

TABLE V: Beam time accounting.

Activity	Time
Commissioning	3 days
Production data taking at $\mathcal{L} = 2 \times 10^{35}$ cm^{-2} sec^{-1}	100 days
Target anneals and/or target change	4 days
Calibration runs on ^{12}C and empty target	10 days
Møller polarimeter runs	3 days
Total	120 days

tainties for the asymmetry can be significantly reduced by appropriate event selection cuts. Most of the techniques and equipment suggested in this proposal have been successfully used in previous CLAS experiments described in Ref. [9] and in Section IV.

We believe that the measurements we intend to carry out in this proposal, combined with the experiments to measure beam spin asymmetries, are an indispensable prerequisite for the development of the GPD field and therefore of the understanding of the structure of the nucleon.

VII. CONCLUSIONS

In summary, we propose to perform two DVCS experiments using the basic equipment of CLAS12 with an 11 GeV beam:

- the first experiment will use a total of **80 days of polarized beam time** on the CLAS12 LH_2 target in order to measure the **DVCS beam spin asymmetry** over a unprecedented range of x_B (down to 0.1, up to 0.7), Q^2 (up to 9 GeV^2) and t;
- the second experiment will use a total of **120 days of beam time on the CLAS12 polarized ammonia target** in order to measure the **DVCS target spin asymmetry** in the same kinematical domain.

Both these data sets, along with other cross section measurements from Hall A and other experiments world-wide will contribute to perfecting our knowledge of GPDs, through a global fit of parametrized GPDs. There is no doubt that Jefferson Lab, with an 11 GeV electron beam, will make the most significant impact on our knowledge of the nucleon structure through the study of GPDs.

With such a wide t and Q^2 coverage, it will be possible to study the onset of twist-3 (and higher) effects which enter the BSA and TSA with at least an additional power of $\sqrt{-t}/Q$. Moreover, we would like to point out that having information on both the BSA and TSA in the same range of (x_B, t, Q^2), which are *mostly* sensitive to the GPD H (for the BSA) and to both H and $\widetilde{H}$ (for the TSA), should allow us to somewhat separate the contributions from both GPDs. Last but not least, during the BSA experiment, we will also be able to extract difference of cross sections and total cross sections with systematic errors of the order 10%, in a wide kinematical range.

Note that the beam time requested in these proposals can be shared with other proposed experiments such as the deeply virtual pseudo-scalar meson electroproduction (unpolarized target part) and polarized structure function (polarized target part), examined by this PAC.

Finally, we would like to point out that extensions of these experiments are very likely to follow in subsequent 12 GeV PACs: the same setup used for the BSA measurement, except for the target material, can be used to investigate DVCS on deuterium, both for coherent DVCS on the deuteron and for DVCS on the quasi-free neutron as detailed in Appendix A.

APPENDIX A: POTENTIAL EXTENSIONS OF DVCS EXPERIMENTS

We would like to point out that extensions of the experiments proposed in this document are very likely to follow in subsequent 12 GeV PACs: the same setup used for the BSA measurement, except for the target material. The interest is two-fold:

- $ed \to ed\gamma$ (coherent DVCS) would allow the first investigation of GPDs for a spin-1 object. In thise case, 9 GPDs may be defined, but can also be linked within some approximations to the nucleon GPDs.

- $e(n) \to en\gamma$ (quasi-free DVCS on the neutron) is of primary importance since in this case, Eq. (22) is dominated by the contribution from the GPD E, which is essentially unknown and enters Ji's sum rule on equal footings with H. In this case, the outgoing neutron would be detected, both in the forward EC and in the central detector, where additional thick sincillators could be inserted between the TOF counters and the solenoid cryostat.

APPENDIX B: TECHNICAL PARTICIPATION OF RESEARCH GROUPS

1. DAPNIA/SPhN-Saclay, France

The DAPNIA/SPhN-Saclay group is actively involved in this proposal, as well as in one other proposal using CLAS12, and one other proposal for Hall A.

Among CLAS12 baseline equipment, the group intends to take responsibility for the design, prototyping, construction and testing of the central tracker (both the cylindrical part and the forward part). The group has started working on an option based on cylindrical Micromegas detectors. Provided this is shown to work as designed, the group anticipates that this option will be examined in comparison with the Silicon Strip tracker, toward the end of 2007 or the beginning of 2008. Four research staff members and four technicians/engineers are likely to work at least part time on this project in the next few years. Funding for the group is from CEA-France. Additional sources of funding (ANR-France, European Union 7th PCRD) will be sought as appropriate.

In case the Micromegas option is not suitable, or not selected for valid reasons, the group would study other technical participations in the CLAS12 baseline equipment.

Beyond the baseline equipment, the group is also interested in exploring neutral particle detection (mostly neutrons) in the central detector of CLAS12, in the so far empty space between TOF scintillators and solenoid cryostat.

2. Fairfield University

Fairfield University is actively involved in the DVCS proposal as well as other CLAS12 proposals. Fairfield University is planning to contribute to the development of the CLAS12 software such as the GEANT4 simulation. Fairfield University is also planning to recruit undergraduate students which can work on hardware projects over the summer at the Laboratory or in collaboration with other groups.

3. Kyungpook National University, Republic of Korea

Kyungpook National University group has been actively participating in the CLAS collaboration. The group has been contributing to the laser calibration of the TOF system and playing a central role of developing the prototype for the 12 GeV TOF central detector. The group commits to design, construct, test, and maintainance of the 12 GeV TOF central detector. The group also intends to participate in the data analysis.

4. University of Glasgow, United Kingdom

The Glasgow Univ. group is actively involved in this proposal, as well as in another proposal using CLAS12, one proposal for Hall A and the GlueX proposal.

The Glasgow group plans to contribute to the design, prototyping, construction and testing of the following CLAS12 baseline equipment: silicon vertex tracker electronic readout system, data acquisition, GRID computing, photon beamline. Beyond the baseline equipment, the group is also interested in building a RICH detector for kaon identification in CLAS12.

Seven faculty members and research staff and four technicians/engineers are likely to work at least part time on this project in the next few years. Funding for the group is from the UK Engineering and Physical Sciences Research Council, EPSRC. Additional sources of

funding will be sought as appropriate.

5. University of New Hampshire

The University of New Hampshire Nuclear Physics group is actively involved in this proposal, as well as three other proposal using CLAS12.

The UNH group is committed to significant contributions in the development of the CLAS12 software. Maurik Holtrop is currently chair of the CLAS12 GEANT4 simulation group to which our post-doc Hovanes Egiyan is also contributing. Since currently the main software efforts for CLAS12 are in the area of simulation we are also part of and contributing to the general CLAS12 Software group. Current manpower commitments to this effort are 0.15 FTE of a faculty and 0.4 FTE of one post-doc. We expect to increase this effort as our CLAS activities wind down and our CLAS12 activities pick up and we expect to attract some talented undergraduate students to this project.

Among CLAS12 baseline equipment, the group intends to take responsibility for the design, prototyping, construction and testing of the silicon vertex detector and perhaps the inner detector's silicon tracking detectors. Faculty member Maurik Holtrop is likely to work at least part time on this project in the next few years and is likely to be joined by Jim Connel, a cosmic ray experimentalist with a background in nuclear physics, who is very interested in joining the vertex detector project. He has considerable experience with silicon detectors for space observations. Funding for the group is from DOE and additional sources of funding will be sought for this project to bring aboard Prof. Connel. If funded we are likely to attract a post-doc, a graduate student and one or two undergraduate students to this project.

Beyond the baseline equipment, the group is also interested in exploring an extended inner calorimeter for CLAS12.

[1] X.-D. Ji, Phys. Rev. **D55**, 7114 (1997), hep-ph/9609381.

[2] X.-D. Ji, Phys. Rev. Lett. **78**, 610 (1997), hep-ph/9603249.

[3] A. V. Radyushkin, Phys. Lett. **B380**, 417 (1996), hep-ph/9604317.

[4] A. V. Radyushkin, Phys. Rev. **D56**, 5524 (1997), hep-ph/9704207.

[5] S. Stepanyan et al. (CLAS), Phys. Rev. Lett. **87**, 182002 (2001), hep-ex/0107043.

[6] A. Airapetian et al. (HERMES), Phys. Rev. Lett. **87**, 182001 (2001), hep-ex/0106068.

[7] P. Bertin, C. Hyde-Wright, R. Ransome, F. Sabatié, et al. (Hall A), JLab Experiment E00-110 (2000).

[8] V. Burkert, L. Elouadrhiri, M. Garçon, and S. Stepanyan (CLAS), JLab Experiment E01-113 (2001).

[9] S. Chen, H. Avakian, V. Burkert, and P. Eugenio (the CLAS) (2006), hep-ex/0605012.

[10] X.-D. Ji, W. Melnitchouk, and X. Song, Phys. Rev. **D56**, 5511 (1997), hep-ph/9702379.

[11] A. V. Belitsky, D. Mueller, and A. Kirchner, Nucl. Phys. **B629**, 323 (2002), hep-ph/0112108.

[12] M. Kopytin (HERMES), AIP Conf. Proc. **792**, 424 (2005).

[13] G. Gavalyan et al. (CLAS), CLAS-ANALYSIS note in review (2006).

[14] H. Avakian et al. (CLAS), CLAS-ANALYSIS note in review (2006).

[15] P. Bertin, C. Hyde-Wright, F. Sabatié, E. Voutier, et al. (Hall A), JLab Experiment E03-116 (2003).

[16] A. Biselli, L. Elouadrhiri, K. Joo, and S. Niccolai (CLAS), JLab Experiment E05-114 (2005).

[17] V. Burkert, L. Elouadrhiri, M. Garçon, R. Niyazov, and S. Stepanyan (CLAS), JLab Experiment E06-003 (2003).

[18] N. d'Hose, E. Burtin, P. A. M. Guichon, and J. Marroncle, Eur. Phys. J. **A19**, Suppl147 (2004).

[19] R. Niyazov and S. Stepanyan (CLAS), CLAS-NOTE 2005-021 (2005).

[20] F.-X. Girod and M. Garçon (CLAS), CLAS-NOTE 2005-001 (2005).

[21] F.-X. Girod (CLAS), CLAS-NOTE 2005-023 (2005).

[22] V. Kubarovsky, Communication to the DVCS working group, unpublished (2006).

[23] L. Elouadrhiri, An overview of the CLAS12 spectrometer (2006).

[24] C. D. Keith et al., Nucl. Instrum. Meth. **A501**, 327 (2003).

[25] M. Mestayer, K. Mikhaylov, H. Avakian, et al., FastMC fast detector simulation program for CLAS12, unpublished (2006).

[26] H. Avakian, clas12DVCS computer program for DVCS/BH and single π^0 event simulations, unpublished (2005).

[27] M. Vanderhaeghen, M. Guidal, P. Guichon, and L. Mossé, Computer Codes for DVCS and BH Calculations, Private Communications (2006).

[28] M. Vanderhaeghen, P. A. M. Guichon, and M. Guidal, Phys. Rev. **D60**, 094017 (1999), hep-ph/9905372.

[29] J. Pumplin et al., JHEP **07**, 012 (2002), hep-ph/0201195.

[30] A. D. Martin, R. G. Roberts, W. J. Stirling, and R. S. Thorne, Eur. Phys. J. **C28**, 455 (2003), hep-ph/0211080.